

LINKING GHOST PENALTY AND AGGREGATED UNFITTED METHODS

SANTIAGO BADIA^{1,2,*}, ERIC NEIVA², AND FRANCESC VERDUGO²

ABSTRACT. In this work, we analyse the links between ghost penalty stabilisation and aggregation-based discrete extension operators for the numerical approximation of elliptic partial differential equations on unfitted meshes. We explore the behavior of ghost penalty methods in the limit as the penalty parameter goes to infinity, which returns a strong version of these methods. We observe that these methods suffer locking in that limit. On the contrary, aggregated finite element spaces are locking-free because they can be expressed as an extension operator from well-posed to ill-posed degrees of freedom. Next, we propose novel ghost penalty methods that penalise the distance between the solution and its aggregation-based discrete extension. These methods are locking-free and converge to aggregated finite element methods in the infinite penalty parameter limit. We include an exhaustive set of numerical experiments in which we compare weak (ghost penalty) and strong (aggregated finite elements) schemes in terms of error quantities, condition numbers and sensitivity with respect to penalty coefficients on different geometries, intersection locations and mesh topologies.

Keywords: Embedded methods; unfitted finite elements; stabilisation techniques; ghost penalty; aggregated finite elements.

1. INTRODUCTION

Standard finite element methods (FEMs) requires cumbersome and time-consuming body-fitted mesh generation, which is hard to automatise and does not scale properly on distributed platforms. These methods are not suitable for problems with moving boundaries or interfaces. Conversely, unfitted FEMs provide a great amount of flexibility at the geometrical discretisation step. They can embed the domain of interest in a geometrically simple background grid (usually a uniform or an adaptive Cartesian grid), which can be generated and partitioned much more efficiently. Analogously, they can easily capture embedded interfaces. As a result, unfitted finite element (FE) methods are generating interest in applications with moving interfaces, such as fracture mechanics [1, 2], fluid-structure interaction [3, 4, 5, 6], two-phase and free surface flows [7, 8], localised plastic deformation [9], and in applications with varying domains, such as shape or topology optimisation [10], additive manufacturing [11, 12], and stochastic geometry problems [13]. In the numerical community, this family of methods is known by different names, e.g., *unfitted*, *embedded*, *immersed*. Besides, many different schemes have been proposed; see, e.g. the extended finite element method (XFEM) [14], the cutFEM method [15], the aggregated finite element method (AgFEM) [16], the cutIGA method [17], the immersed boundary method [18], the finite cell method [19], the shifted boundary method [20], the immersogeometric method [21], the Cartesian grid FEM [22] and discontinuous Galerkin (DG) methods with cell aggregation [23, 24, 25, 26].

In the case of unfitted boundaries, unfitted methods lead to unstable and severe ill-conditioned discrete problems [27, 16], unless a specific technique mitigates the problem. The intersection of a background cell with the physical domain can be arbitrarily small and with unbounded aspect ratio. It leads to the *small cut cell problem*; FE shape functions on the background (unfitted) mesh can have arbitrarily small support in the physical domain. This support depends on the intersection between the background mesh and the boundary (or interface), which in general cannot be controlled. This problem is also present on unfitted interfaces with a high contrast of physical properties [28].

Despite vast literature on the topic (see, e.g., [29, 30, 31, 32] and the references above), few formulations are fully robust and optimal regardless of cut location and material contrast. The ill-conditioning issue was addressed by the introduction of the so-called *ghost penalty* (GP). In the original article [33], two variants

¹ School of Mathematics, Monash University, Clayton, Victoria, 3800, Australia.

² Centre Internacional de Mètodes Numèrics en Enginyeria, Esteve Terrades 5, E-08860 Castelldefels, Spain.

* Corresponding author.

E-mails: santiago.badia@monash.edu (SB) eneiva@cimne.upc.edu (EN) fverdugo@cimne.upc.edu (FV).

of the methods were originally proposed: (1) A bulk penalty term that penalised the distance between the finite element solution in a patch and a polynomial of the order of the approximation; (2) a face penalty term that penalised normal derivatives of the function (up to the order of approximation) on faces that were in touch with cut cells. The face-based GP has been the method of choice in the so-called CutFEM framework [15]. These schemes were originally motivated for C^0 finite element spaces on simplicial meshes and later used in combination with discontinuous Galerkin formulations.

The so-called *cell aggregation* or *cell agglomeration* techniques are an alternative way to ensure robustness with respect to cut location. This approach is very natural in DG methods, as they can be easily formulated on agglomerated meshes [34, 29, 35], and the method is robust if each cell (now an aggregate of cells) has *enough* support in the interior of the domain [26]. However, the application of these ideas to C^0 Lagrangian finite elements is more involved. The question is how to keep C^0 continuity after the agglomeration.

This problem was addressed in [16], and the resulting method was coined AgFEM. AgFEM combines an aggregation strategy with a map that assigns to every geometrical entity (e.g., vertex, edge, face) one of the aggregates containing it. With these two ingredients, AgFEM constructs a *discrete extension operator* from well-posed degrees of freedom (DOFs) (i.e., the ones related to shape functions with enough support in the domain interior) to ill-posed DOFs (i.e., the ones with small support) that preserves continuity. As a result, the basis functions associated with badly cut cells are removed and the ill-conditioning issues solved. The formulation enjoys good numerical properties, such as stability, condition number bounds, optimal convergence, and continuity with respect to data; detailed mathematical analysis of the method is included in [16] for elliptic problems and in [36] for the Stokes equation. AgFEM is amenable to arbitrarily complex 3D geometries, distributed implementations for large scale problems [37], error-driven h -adaptivity and parallel tree-based meshes [38], explicit time-stepping for the wave equation [39] and elliptic interface problems with high contrast [28].

In this work, we aim to explore the links between the *weak* ghost penalty strategy and the *strong* aggregation-based strategy. In order to do this, we analyse the *strong* form limit of GP methods. In this process, we discuss the *locking* phenomenon of current GP methods. Next, we make use of the AgFEM machinery to define new GP formulations that converge to the classical (strong) AgFEM and thus, are locking-free. We propose two alternative expressions of the penalty method. The stabilisation term penalises the distance between the solution and its interpolation onto the AgFEM space. This distance can be expressed using a weighted L^2 product or an H^1 product.

This work is structured as follows. We introduce the geometrical discretisation in Section 2 and the problem statement in Section 3, which include notations and definitions that are required to implement GP and AgFEM. Next, we introduce some GP formulations and analyse their *strong* limit in Section 4. After that, we present the AgFEM and its underlying discrete extension operator in Section 5. In this section, we propose a new family of GP methods that are a weak version of AgFEM. We comment on the implementation aspects of all the methods in Section 6. In Section 7, we provide a detailed comparison of all these different schemes, in terms of accuracy and condition number bounds, for different values of the penalty parameter, geometries, and intersection locations. We consider Poisson and linear elasticity problems on isotropic and anisotropic meshes. We draw some conclusions in Section 8. The original contributions of the article are:

- (1) A discussion about the links between strong (AgFEM) and weak (GP) methods for solving the ill-conditioning of C^0 Lagrangian unfitted finite element methods;
- (2) A discussion about the locking phenomenon of GP strategies in the strong limit and corrective measures;
- (3) Design and analysis of GP schemes that are a weak versions of AgFEM and locking-free;
- (4) A thorough numerical experimentation comparing GP methods and strong discrete extension methods in terms of error quantities, condition numbers, sensitivity with respect to penalty coefficients, etc.

2. GEOMETRICAL DISCRETISATION

Let us consider an open bounded polyhedral Lipschitz domain $\Omega \subset \mathbb{R}^d$, d being the space dimension, in which we pose our partial differential equation (PDE). Standard FE methods rely on a geometrical

discretisation of Ω in terms of a partition of the domain (or an approximation of it). This step involves so-called unstructured mesh generation algorithms. The resulting partition is a *body-fitted* mesh of the domain. Embedded discretisation techniques alleviate geometrical constraints, because they do not rely on body-fitted meshes. Instead, these techniques make use of a background partition \mathcal{T}_h of an arbitrary artificial domain Ω_h^{art} such that $\Omega \subset \Omega_h^{\text{art}}$. The artificial domain can be trivial, e.g., it can be a bounding box of Ω . Thus, the computation of \mathcal{T}_h is much simpler (and cheaper) than a body-fitted partition of Ω . For simplicity, we assume that \mathcal{T}_h is conforming, quasi-uniform and shape-regular; we represent with h_T the diameter of a cell $T \in \mathcal{T}_h$ and define the characteristic mesh size $h \doteq \max_{T \in \mathcal{T}_h} h_T$. We refer to [38] for the extension to non-conforming meshes.

The definition of unfitted FE discretisations requires some geometrical classifications of the cells in the background mesh \mathcal{T}_h and their *n-faces*. We use *n-face* to denote entities in any dimension. E.g., in 3D, 0-faces are vertices, 1-faces are edges, 2-faces are faces and 3-faces are cells. We use *facet* to denote an *n-face* of dimension $D-1$, i.e., an edge in 2D and a face in 3D.

The cells in the background partition with null intersection with Ω are *exterior* cells. The set of exterior cells $\mathcal{T}_h^{\text{out}}$ is not considered in the functional discretisation and can be discarded. $\mathcal{T}_h^{\text{act}} \doteq \mathcal{T}_h \setminus \mathcal{T}_h^{\text{out}}$ is the *active* mesh. E.g., the XFEM relies on a standard FE space on $\mathcal{T}_h^{\text{act}}$. Unfortunately, the resulting discrete system can be singular (see the discussion below). This problem, a.k.a. *small cut cell problem*, is due to cells with arbitrarily small support on Ω . This fact motivates the further classification of cells in $\mathcal{T}_h^{\text{act}}$. Let $\mathcal{T}_h^{\text{in}}$ be the subset of cells in Ω and $\mathcal{T}_h^{\text{cut}}$ the cut cells (see Figure 1).¹ The interior of $\bigcup_{T \in \mathcal{T}_h^{\#}} T$ is represented with $\Omega_h^{\#}$ for $\# \in \{\text{act}, \text{in}, \text{cut}\}$.

Some of the methods below require the definition of *aggregates*. Let us consider $\mathcal{T}_h^{\text{ag}}$ (usually called an agglomerated or aggregated mesh) obtained after a cell aggregation of $\mathcal{T}_h^{\text{act}}$, such that each cell in $\mathcal{T}_h^{\text{in}}$ only belongs to one aggregate and each aggregate only contains one cell in $\mathcal{T}_h^{\text{in}}$ (the root cell). Based on this definition, cell aggregation only acts on the boundary; interior cells that are not in touch with ill-posed cells remain the same after aggregation. Let $\mathcal{T}_h^{\partial, \text{ag}} \doteq \mathcal{T}_h^{\text{ag}} \setminus \mathcal{T}_h^{\text{in}}$ be the non-trivial aggregates on the boundary (see Figure 1). We refer the interested reader to [16] for the definition of cell aggregation algorithms. The aggregation has been extended to non-conforming meshes in [38] and interface problems in [28], and its parallel implementation described in [37]. It is essential for convergence to minimise the aggregate size in these algorithms. In particular, the characteristic size of an aggregated cell must be proportional to the one of its root cell. The motivation of the cell aggregation is to end up with a new partition in which all cells (aggregates) have support in Ω away from zero, are connected and are shape-regular.

We represent with $C_h^{\#}$ the (simplicial or hexahedral) *exact complex* of $\mathcal{T}_h^{\#}$ for $\# \in \{\text{act}, \text{in}, \text{out}\}$, i.e., the set of all *n-faces* of cells in $\mathcal{T}_h^{\#}$. C_h^{ag} is the subset of *n-faces* in C_h^{act} that lay on the boundaries of aggregates in $\mathcal{T}_h^{\text{ag}}$. We also define the set of *ghost boundary facets* $\mathcal{F}_h^{\text{gh}, \text{cut}}$ as the facets in C_h^{cut} that belong to two active cells in $\mathcal{T}_h^{\text{act}}$ (cut or not). $\mathcal{F}_h^{\text{gh}, \text{ag}} \doteq \mathcal{F}_h^{\text{gh}, \text{cut}} \setminus C_h^{\text{ag}}$ is the subset of these facets that do not lay on aggregate boundaries, see Figure 1.

3. PROBLEM STATEMENT

Let us consider first the Poisson equation in Ω with Dirichlet boundary conditions on $\Gamma_D \subset \partial\Omega$ and Neumann boundary conditions on $\Gamma_N \doteq \partial\Omega \setminus \Gamma_D$. After scaling with the diffusion term, the equation reads: *find* $u \in H^1(\Omega)$ *such that*

$$-\nabla \cdot \nabla u = f \quad \text{in } H^{-1}(\Omega), \quad u = g \quad \text{in } H^{1/2}(\Gamma_D), \quad \mathbf{n} \cdot \nabla u = q \quad \text{in } H^{-\frac{1}{2}}(\Gamma_N), \quad (1)$$

where f is the source term, g is the prescribed value on the Dirichlet boundary and q the prescribed flux on the Neumann boundary.

The following presentation readily applies to other second-order elliptic problems. In particular, we will also consider the linear elasticity problem: *find* $\mathbf{u} \in \mathbf{H}^1(\Omega)$ *such that*

$$-\nabla \cdot \boldsymbol{\sigma}(\mathbf{u}) = \mathbf{f} \quad \text{in } \mathbf{H}^{-1}(\Omega), \quad \mathbf{u} = \mathbf{g} \quad \text{in } \mathbf{H}^{1/2}(\Gamma_D), \quad \mathbf{n} \cdot \boldsymbol{\sigma}(\mathbf{u}) = \mathbf{q} \quad \text{in } \mathbf{H}^{-\frac{1}{2}}(\Gamma_N), \quad (2)$$

¹One can consider a more subtle classification as follows. For any cell $T \in \mathcal{T}_h$, we define the quantity $\eta_T \doteq \frac{|T \cap \Omega|}{|T|}$, $|\cdot|$ being the measure of the set. For a given threshold $\eta_0 \in (0, 1]$, we classify cells $T \in \mathcal{T}_h^{\text{act}}$ as *well-posed* if $\eta_T \geq \eta_0$ and *ill-posed* otherwise. The interior-cut classification is recovered for $\eta_0 = 1$. In any case, the following discussion applies verbatim.

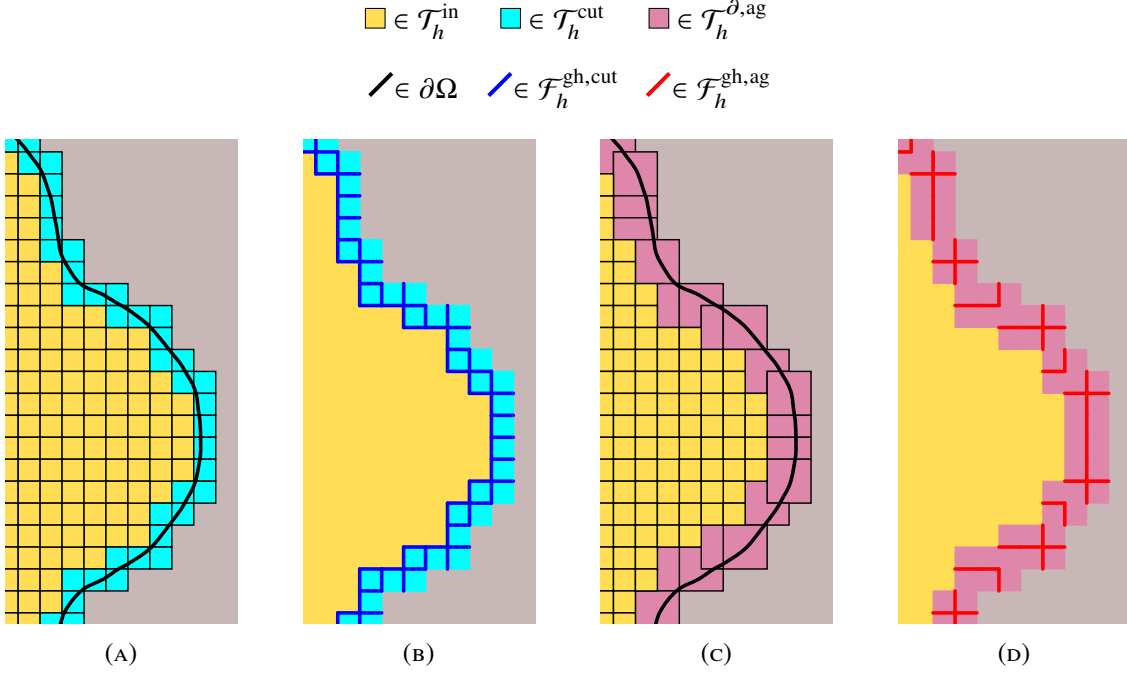


FIGURE 1. Illustration of the main geometrical sets introduced in Sect. 2.

where $\boldsymbol{\epsilon}, \boldsymbol{\sigma} : \Omega \rightarrow \mathbb{R}^{d,d}$ are the strain tensor $\boldsymbol{\epsilon}(\mathbf{u}) \doteq \frac{1}{2}(\nabla \mathbf{u} + \nabla \mathbf{u}^T)$ and stress tensor $\boldsymbol{\sigma}(\mathbf{u}) = 2\mu\boldsymbol{\epsilon}(\mathbf{u}) + \lambda \text{tr}(\boldsymbol{\epsilon}(\mathbf{u}))\mathbf{Id}$; \mathbf{Id} denotes the identity matrix in \mathbb{R}^d . (μ, λ) are the Lamé coefficients. We consider the Poisson ratio $\nu \doteq \lambda/(2(\lambda + \mu))$ is bounded away from $1/2$, i.e. the material is compressible. Since $\lambda = 2\nu\mu/(1 - 2\nu)$, λ is bounded above by μ , i.e. $\lambda \leq C\mu$, $C > 0$.

The simplification of the geometrical discretisation, in turn, complicates the functional discretisation. Standard (body-fitted) FEMs cannot be straightforwardly used. First, the strong imposition of Dirichlet boundary conditions relies on the fact that the mesh is body-fitted. In an embedded setting, Dirichlet boundary conditions are weakly imposed instead. Second, the cell-wise integration of the FE forms is more complicated; integration must be performed on the intersection between cells and Ω only. Third, naive discretisations can be arbitrarily ill-posed.

Let $\mathcal{V}_h^{\text{act}}$ be a standard Lagrangian FE space on $\mathcal{T}_h^{\text{act}}$. As stated above, we consider a weak imposition of boundary conditions with Nitsche's method [16, 19, 15]. This approach provides a consistent numerical scheme with optimal convergence for arbitrary order FE spaces. According to this, we approximate the Poisson problem in (1) with the Galerkin method: find $u_h \in \mathcal{V}_h^{\text{act}}$ such that $a_h(u_h, v_h) = b_h(v_h)$ for any $v_h \in \mathcal{V}_h^{\text{act}}$, with

$$\begin{aligned} a_h(u_h, v_h) &\doteq \int_{\Omega} \nabla u_h \cdot \nabla v_h \, d\Omega + \int_{\Gamma_D} (\tau u_h v_h - u_h (\mathbf{n} \cdot \nabla v_h) - v_h (\mathbf{n} \cdot \nabla u_h)) \, d\Gamma, \quad \text{and} \\ b_h(v_h) &\doteq \int_{\Omega} f v_h \, d\Omega + \int_{\Gamma_D} (\tau g v_h - (\mathbf{n} \cdot \nabla v_h) g) \, d\Gamma + \int_{\Gamma_N} q v_h \, d\Gamma, \end{aligned} \quad (3)$$

with \mathbf{n} being the outward unit normal on $\partial\Omega$. In the case of the linear elasticity problem in (2), the bilinear form and linear functional read:

$$\begin{aligned} a_h(\mathbf{u}_h, \mathbf{v}_h) &\doteq \int_{\Omega} \boldsymbol{\sigma}(\mathbf{u}_h) : \boldsymbol{\epsilon}(\mathbf{v}_h) \, d\Omega + \int_{\Gamma_D} (\tau \mathbf{u}_h \cdot \mathbf{v}_h - \mathbf{n} \cdot \boldsymbol{\sigma}(\mathbf{v}_h) \cdot \mathbf{u}_h - \mathbf{n} \cdot \boldsymbol{\sigma}(\mathbf{u}_h) \cdot \mathbf{v}_h) \, d\Gamma, \quad (4) \\ b_h(\mathbf{v}_h) &\doteq \int_{\Omega} \mathbf{f} \cdot \mathbf{v}_h \, d\Omega + \int_{\Gamma_D} (\tau \mathbf{g} \cdot \mathbf{v}_h - \mathbf{n} \cdot \boldsymbol{\sigma}(\mathbf{v}_h) \cdot \mathbf{g}) \, d\Gamma + \int_{\Gamma_D} \mathbf{q} \cdot \mathbf{v}_h \, d\Gamma. \end{aligned}$$

We note that the second term in all the forms above are associated with the weak imposition of Dirichlet boundary conditions with Nitsche's method [40].² Stability of Lagrangian FEMs relies, e.g., for the

²Other weak imposition of boundary conditions involve the penalty method or a non-symmetric version of Nitsche's method [41]. In any case, the penalty formulation is not weakly consistent for higher order methods and the non-symmetric formulation breaks the symmetry of the system and is not adjoint consistent.

Poisson problem, on the following property:

$$\int_{\Gamma_D \cap T} (\tau_T u_h^2 - 2u_h (\mathbf{n} \cdot \nabla u_h)) \, d\Gamma \leq C \int_{\Gamma_D \cap T} \tau_T u_h^2 \, d\Gamma + \|\nabla u_h\|_{\mathbf{L}^2(T)}^2, \quad \forall T \in \mathcal{T}_h^{\text{cut}} \quad (5)$$

for some $C > 0$ independent of h_T .

A value of τ_T that satisfies (5) can be computed using a cell-wise eigenvalue problem. In shape-regular body-fitted meshes, one can simply use $\tau_T \doteq \beta h_T^{-1}$. Here, $\beta = \tilde{\beta} m^2$, with $\tilde{\beta}$ a *large enough* problem-dependent parameter and m the order of $\mathcal{V}_h^{\text{act}}$, while h_T is the diameter of T . For XFEM, we only have stability over $\|\nabla u_h\|_{\mathbf{L}^2(T \cap \Omega)}^2$ in the right-hand side of (5). In this case, the minimum value of τ_T that makes the problem stable tends to infinity in some cell configurations as $|T \cap \Omega| \rightarrow 0$. As a result, unfitted FEMs like XFEM are not robust to cell cut locations (boundaries or interfaces).

Condition number bounds for the resulting linear system are strongly linked to the stability issue commented above. A shape function of the finite element space ϕ_i must satisfy, in at least one cell $T \in \mathcal{T}_h^{\text{act}}$,

$$C_- h_T^d \leq \int_{T \cap \Omega} \phi_i^2 \, dT \leq C_+ h_T^d, \quad (6)$$

for $C_+ > C_- > 0$ independent of h_T . This condition can be proved for Lagrangian FEs on body-fitted meshes ($T \cap \Omega = T$). It implies that the mass matrix is spectrally equivalent to the identity matrix for quasi-uniform and shape-regular partitions. However, it is obvious to check that this condition fails as $|T \cap \Omega| \rightarrow 0$ since $\int_T \phi_i^2 \, dT \rightarrow 0$. The plain vanilla FEM on the background mesh leads to severely ill-conditioned linear systems. Recent research works have tried to solve this issue at the preconditioner level (see, e.g., [27, 42]).

In the coming sections, we will present methods that solve the previous problems by providing stability over full background mesh cells $T \in \mathcal{T}_h^{\text{act}}$, i.e., T instead of $T \cap \Omega$. With these methods, we can use the same expression of τ_T as in body-fitted meshes, h_T being the background cell size. We will often make abuse of notation, using u_h to refer to both the scalar unknown in (3) and the vector unknown in (4), making distinctions where relevant. We use $A \gtrsim B$ (resp. $A \lesssim B$) to denote $A \geq CB$ (resp. $A \leq CB$) for some positive constant C that does not depend on h and the location of the cell cuts. Uniform bounds irrespectively of boundary or interface locations is the driving motivation behind all these methods.

4. GHOST PENALTY

The ghost penalty formulation was originally proposed in [33] to fix the ill-posedness problems of XFEM discussed above. The method adds a stabilising bilinear form s_h to the formulation that provides an *extended* stability while preserving the convergence rates of the body-fitted method.

Definition 4.1. *Let $n \leq m$, where m is the order of $\mathcal{V}_h^{\text{act}}$, and $\mathcal{E}^n : H^n(\Omega) \rightarrow H^n(\Omega_h^{\text{act}})$ be a continuous extension operator. Let $\mathcal{V}(h) \doteq \mathcal{V}_h^{\text{act}} + H^2(\Omega_h^{\text{act}})$. We endow $\mathcal{V}(h)$ with the extended stability norm:*

$$\|v\|_{\mathcal{V}(h)}^2 \doteq \|\nabla v\|_{\mathbf{L}^2(\Omega_h^{\text{act}})}^2 + \|\tau^{\frac{1}{2}} v\|_{\mathbf{L}^2(\Gamma_D)}^2 + \sum_{T \in \mathcal{T}_h^{\text{act}}} h_T^2 \|v\|_{H^2(T)}^2, \quad \forall u \in \mathcal{V}(h).$$

A suitable GP term s_h for problems (3) and (4) is a positive semi-definite symmetric form that satisfies the following properties uniformly w.r.t. the mesh size h of the background mesh and interface intersection:

(i) *Extended stability:*

$$s_h(u_h, u_h) + \|\nabla u_h\|_{\mathbf{L}^2(\Omega)}^2 \gtrsim \|\nabla u_h\|_{\mathbf{L}^2(\Omega_h^{\text{act}})}^2, \quad \forall u_h \in \mathcal{V}_h^{\text{act}}, \quad (7)$$

(ii) *Continuity:*

$$s_h(u, v_h) \lesssim \|u\|_{\mathcal{V}(h)} \|v_h\|_{\mathcal{V}(h)}, \quad \forall u \in \mathcal{V}(h), v_h \in \mathcal{V}_h^{\text{act}}. \quad (8)$$

(iii) *Weak consistency:*

$$s_h(\mathcal{E}^{n+1}(u), v_h) \lesssim h^n \|u\|_{H^{n+1}(\Omega)} \|v_h\|_{\mathcal{V}(h)}, \quad \forall u \in H^{n+1}(\Omega). \quad (9)$$

Under these conditions, the GP unfitted formulation is well-posed and exhibits optimal convergence rates. The following abstract results have been proved in the literature for specific definitions of s_h that satisfy Def. 4.1. See, e.g., [33, Lem. 4.2, Lem. 4.3, Prop. 4.4], [43, Sect. 4] and [44, Sec. 4]. Note that the norm includes control, not only over $\|\nabla v_h\|_{\mathbf{L}^2(\Omega)}$ (which comes from the standard Laplacian term in the

formulation), but $\|\nabla v_h\|_{L^2(\Omega_h^{\text{act}})}$. This extra stabilisation in (7) is provided by the GP term and essential for well-posedness independent of the boundary location.

Proposition 4.2. *Let s_h satisfy Def. 4.1. It holds:*

$$a_h(u_h, u_h) + s_h(u_h, u_h) \gtrsim \|u_h\|_{\mathcal{V}(h)}^2, \quad a_h(u, v_h) + s_h(u, v_h) \lesssim \|u\|_{\mathcal{V}(h)} \|v_h\|_{\mathcal{V}(h)}, \quad (10)$$

for any $u_h, v_h \in \mathcal{V}_h^{\text{act}}$, $u \in \mathcal{V}(h)$. Thus, there is a unique

$$u_h \in \mathcal{V}_h^{\text{act}} : a_h(u_h, v_h) + s_h(u_h, v_h) = b(v_h), \quad \forall v_h \in \mathcal{V}_h^{\text{act}}. \quad (11)$$

Furthermore, the condition number κ of the resulting linear system when using a standard Lagrangian basis for $\mathcal{V}_h^{\text{act}}$ holds $\kappa \lesssim h^{-2}$.

Proof. The main ingredient is the following trace inequality for continuous functions on cut cells (see [45]):

$$\|\psi\|_{L^2(\partial(\Omega \cap T))}^2 \lesssim h_T^{-1} \|\psi\|_{L^2(\Omega \cap T)}^2 + h_T \|\psi\|_{H^1(\Omega \cap T)}^2, \quad \forall \psi \in H^1(\Omega \cap T), \quad (12)$$

where $\partial(\Omega \cap T)$ is the boundary of $\Omega \cap T$. Using a standard discrete inequality on $\mathcal{T}_h^{\text{act}}$, namely $\|\nabla u_h\|_{H^1(T)} \lesssim h_T^{-1} \|u_h\|_{L^2(T)}$ for any $u_h \in \mathcal{V}_h^{\text{act}}$ and $T \in \mathcal{T}_h^{\text{act}}$, we readily get

$$\|\mathbf{n} \cdot \nabla u_h\|_{L^2(\Gamma_D \cap T)}^2 \lesssim h_T^{-1} \|\nabla u_h\|_{L^2(T)}^2, \quad \forall u_h \in \mathcal{V}_h^{\text{act}}. \quad (13)$$

Using (7), Cauchy-Schwarz and Young inequalities, (13) and the expression for τ , we can prove (5). Thus, the GP provides a stronger coercivity result, namely

$$a(u_h, u_h) + s(u_h, u_h) \gtrsim \|u_h\|_{\mathcal{V}(h)}^2, \quad \forall u_h \in \mathcal{V}_h^{\text{act}},$$

for the same definition of τ that is needed in body-fitted meshes, i.e., the value of β does not depend on the location of the cell cut. Continuity in (10) is obtained invoking (12), the standard inverse inequality $\|\nabla u_h\|_{L^2(T)} \lesssim h_T^{-1} \|u_h\|_{L^2(T)}$ and (8). The cut-independent condition number bound is a by-product of the enhanced coercivity in (10). Using the Poincaré inequality, one can readily prove that $\|u_h\|_{L^2(\Omega_h^{\text{act}})} \lesssim \|u_h\|_{\mathcal{V}(h)}$. Using the inverse inequality on the background mesh and (13) one can prove that $\|u_h\|_{\mathcal{V}(h)} \lesssim h^{-1} \|u_h\|_{L^2(\Omega_h^{\text{act}})}$. Finally, one can use the standard bounds for the mass matrix on the background mesh (6) to prove the result (see, e.g., [33, Lem. 4.3]). \square

Proposition 4.3. *Let m be the order of $\mathcal{V}_h^{\text{act}}$. If $u \in H^{n+1}(\Omega)$, $m \geq n \geq 1$, is the solution of (3) or (4) and $u_h \in \mathcal{V}_h^{\text{act}}$ is the solution of (11), then:*

$$\|u - u_h\|_{\mathcal{V}(h)} \lesssim h^n |u|_{H^{n+1}(\Omega)}, \quad \|u - u_h\|_{L^2(\Omega)} \lesssim h^{n+1} |u|_{H^{n+1}(\Omega)}.$$

Proof. The convergence analysis relies on standard approximation error bounds for $\mathcal{E}^{n+1}(u)$ in $\mathcal{V}_h^{\text{act}}$ and the weak consistency in (8). \square

In the following, we show some definitions of s_h with these properties.

4.1. Bulk ghost penalty (B-GP). The *bulk* ghost penalty stabilisation was originally proposed in [33]. The idea of this formulation is to add the stabilisation term

$$s_h(u_h, v_h) \doteq \sum_{U \in \mathcal{T}_h^{\theta, \text{ag}}} \left(\gamma h_U^{-2} (u_h - \pi_U(u_h)), v_h \right)_U, \quad (14)$$

where $\pi_U(\cdot)$ represents the $L^2(U)$ projection onto the polynomial space $\mathcal{P}_p(U)$ (for simplicial meshes) or $\mathcal{Q}_p(U)$ (for hexahedral meshes). $\gamma > 0$ is a numerical parameter that must be chosen. This method penalises the difference between the restriction of the FE solution in the aggregate and a local polynomial space on the aggregate. Since the aggregate-wise polynomial spaces have enough support in Ω by construction, it provides stability on ill-posed cells.

Proposition 4.4. *The expression of s_h in (14) is a suitable GP stabilisation that satisfies the conditions (7)-(9) in Def. 4.1.*

Proof. The analysis of the B-GP stabilisation, which indirectly proves the conditions in Def. 4.1, can be found in [33, Lem. 4.2, Prop. 4.4]. \square

4.2. Face ghost penalty (F-GP). The most popular ghost stabilisation technique relies on the penalisation of inter-element m normal derivatives on the facets in $\mathcal{F}_h^{\text{gh,cut}}$, where m stands for the FE space order. This is the stabilisation that is being used in the so-called CutFEM framework [15]. Let us consider linear FEs in the following exposition. Given a face $F \in \mathcal{F}_h^{\text{gh,cut}}$ and the two cells K and K' sharing this face, we define $\llbracket \partial_n u \rrbracket \doteq \mathbf{n}_K \cdot \nabla u|_K + \mathbf{n}_{K'} \cdot \nabla u|_{K'}$. h_F is some average of h_K and $h_{K'}$. We define the GP stabilisation term:

$$s_h(u_h, v_h) = \sum_{F \in \mathcal{F}_h^{\text{gh,cut}}} (\gamma h_F \llbracket \partial_n u_h \rrbracket, \llbracket \partial_n v_h \rrbracket)_F. \quad (15)$$

The method weakly enforces C^m continuity across cells as soon as one of the cells is cut. This weak constraint of cut cells also provides the desired extended stability described above.

Proposition 4.5. *The expression of s_h in (14) is a suitable GP stabilisation that satisfies the conditions (7)-(9) in Def. 4.1.*

Proof. The analysis of the F-GP stabilisation can be found in [33, Lem. 4.2, Lem. 4.3, Prop. 4.4] for linear elements and [43, Sect. 4] and [44, Sec. 4] in the general case and applied to linear elasticity problems. \square

4.3. The limit $\gamma \rightarrow \infty$. The GP method underlying idea is to *rigidise* the shape functions on the boundary zone. One question that arises is: what happens when the penalty parameter $\gamma \rightarrow \infty$? Can we use the previous methods in a *strong* way? Can we build spaces that exactly satisfy the constraints in that limit?

Let us consider the F-GP method first. In the limit $\gamma \rightarrow \infty$, the stabilisation term in that case enforces full C^m continuity of the FE solution on $\mathcal{F}_h^{\text{gh,cut}}$. The only functions in $\mathcal{V}_h^{\text{act}}$ that satisfy this continuity are *global* polynomials in Ω_h^{cut} . As a result, the method is not an accurate method that converges to the exact solution as $h \rightarrow 0$.

Let us look at the B-GP now. In the limit $\gamma \rightarrow \infty$, the solution must be a piecewise C^0 polynomial on the aggregated mesh $\mathcal{T}_h^{\text{ag}}$. The limit constraint is weaker than the one for F-GP. However, it is still too much to eliminate the locking phenomenon in general. In order to satisfy exactly the penalty term, the aggregate values are polynomial extensions of the root cell polynomials. In general, these extensions do not satisfy C^0 continuity (Aggregates are not tetrahedra or hexahedra anymore, but an aggregation of these polytopes that can have more general shapes, e.g., L-shaped.) As a result, the B-GP term is not just constraining the values of the ill-posed cell (as one could expect) but the ones of the well-posed cells too. Furthermore, these constraints are not local but can propagate across multiple aggregates, depending on the mesh topology.

The previous observations motivate a slight improvement of F-GP (CutFEM). Instead of considering the face penalty on all faces in $\mathcal{F}_h^{\text{gh,cut}}$, one can only penalise the subset of intra-aggregate faces $\mathcal{F}_h^{\text{gh,ag}}$:

$$s_h(u_h, v_h) = \sum_{F \in \mathcal{F}_h^{\text{gh,ag}}} (\gamma h_F \llbracket \partial_n u_h \rrbracket, \llbracket \partial_n v_h \rrbracket)_F. \quad (16)$$

It is easy to check that this variant (16) of the F-GP method, referred to as **intra-aggregate ghost penalty (A-GP)**, has the same behaviour in the limit as the bulk one, i.e., it is still affected by locking. The analysis in this case readily follows from Prop. 4.5.

5. AGGREGATED FINITE ELEMENTS

The natural question that arises from this discussion is: how can we define a strong version of the GP stabilisation that is free of the *locking* described above? The answer to this question was the AgFEM proposed in [16]. The underlying idea of this method is to define a new FE space that can be expressed in terms of an aggregate-wise *discrete extension* operator $\mathcal{E}_h^{\text{ag}} : \mathcal{V}_h^{\text{in}} \rightarrow \mathcal{V}_h^{\text{act}}$ that extends FE functions from the root cells to the cut cells. This definition solves two problems: the non-locality of the constraints and the constraining of interior cells DOFs. The image of this extension is the aggregated finite element (AgFE) space $\mathcal{V}_h^{\text{ag}} \subset \mathcal{V}_h^{\text{act}}$; $\mathcal{V}_h^{\text{ag}}$ can be built by adding constraints to $\mathcal{V}_h^{\text{act}}$. The new AgFE space is not affected by the small cut cell problem, since the ill-posed DOFs are constrained by well-posed interior DOFs.

Since $\mathcal{V}_h^{\text{act}}$ is a nodal Lagrangian FE space, there is a one-to-one map between shape functions, nodes and DOFs. For each node in the mesh, we can define its owner as the lowest dimensional n-face (e.g., vertex, edge, face, cell) that contains it, to create a map $O_h^{\text{dof} \rightarrow \text{nf}}$. We define the set of ill-posed DOFs as

the ones owned by cut/external n-faces, i.e., $C_h^{\text{cut}} \setminus C_h^{\text{in}}$. The rationale for this definition is the fact that the shape functions associated to these DOFs are the ones that can have an arbitrarily small support on Ω .

The definition of the discrete extension operator in the AgFEM requires to define an ownership map $O_h^{\text{nf} \rightarrow \text{ag}} : C_h^{\text{cut}} \setminus C_h^{\text{in}} \rightarrow \mathcal{T}_h^{\delta, \text{ag}}$ from ill-posed cut/external n-faces to aggregates. This mapping is not unique for inter-aggregate DOFs and can be arbitrarily chosen. On the other hand, each aggregate has a unique root cell in $\mathcal{T}_h^{\text{in}}$. Composing all these maps, we end up with an ill-posed to root cell map $O_h^{\text{dof} \rightarrow \text{in}} : C_h^{\text{cut}} \setminus C_h^{\text{in}} \rightarrow \mathcal{T}_h^{\text{in}}$.

Let $O_h^{\text{nf} \rightarrow \text{dof}}$ be the inverse of $O_h^{\text{dof} \rightarrow \text{nf}}$, i.e., the map that returns the DOFs owned by an n-face in C_h^{act} . We also need a *closed* version $\bar{O}_h^{\text{nf} \rightarrow \text{dof}}$ of this ownership map, which given an n-face C in C_h^{act} returns the owned DOFs of all n-faces $C' \in C_h^{\text{act}}$ in the closure of C , $C' \subset C$. $\bar{O}_h^{\text{nf} \rightarrow \text{dof}}$ is the map that describes the *locality* of FE methods. The only DOFs that are *active* in a cell $T \in \mathcal{T}_h^{\text{act}}$ are the ones in $\bar{O}_h^{\text{nf} \rightarrow \text{dof}}(T)$. Analogously, only the shape functions associated to these DOFs have support on T .

We are in position to define the discrete extension operator as follows. An ill-posed DOF in $C_h^{\text{cut}} \setminus C_h^{\text{in}}$ is computed as a linear combination of the well-posed DOFs in the closure of the root cell that owns it. Using the notation introduced so far, these DOFs are the ones in $O_h^{\text{ipd} \rightarrow \text{wpd}} \doteq \bar{O}_h^{\text{nf} \rightarrow \text{dof}} \circ O_h^{\text{dof} \rightarrow \text{in}}$. In particular, the value of $\sigma^\alpha \in C_h^{\text{cut}} \setminus C_h^{\text{in}}$ is computed as follows

$$\sigma^\alpha(\cdot) = \sum_{\sigma^\beta \in O_h^{\text{ipd} \rightarrow \text{wpd}}(\alpha)} \sigma^\alpha(\phi^\beta) \sigma^\beta(\cdot) = \sum_{\sigma^\beta \in O_h^{\text{ipd} \rightarrow \text{wpd}}(\alpha)} \phi^\beta(\mathbf{x}^\alpha) \sigma^\beta(\cdot). \quad (17)$$

We can readily check that this expression extends the well-posed DOF values on interior cells to the ill-posed DOF values that only belong to cut cells. The application of (17) to a FE function in $\mathcal{V}_h^{\text{in}}$ provides the sought-after discrete extension operator $\mathcal{E}_h^{\text{ag}}$ and the AgFE space $\mathcal{V}_h^{\text{ag}}$.³

The implementation of AgFEM simply requires the imposition of the constraints in (17). These constraints are cell-local (much simpler than the ones in h -adaptive mesh refinement). On the other hand, the method does not require any modification of the forms in (3)-(4). Instead, it is the FE space the one that changes. The method reads: find $u_h \in \mathcal{V}_h^{\text{ag}}$ such that $a(u_h, v_h) = b(v_h)$ for any $v_h \in \mathcal{V}_h^{\text{ag}}$. The key properties of the AgFEM are:

$$\|\nabla u_h\|_{L^2(\Omega_h^{\text{act}})}^2 \lesssim \|\nabla u_h\|_{L^2(\Omega)}^2, \quad \|u_h\|_{L^2(\Omega_h^{\text{act}})}^2 \lesssim \|u_h\|_{L^2(\Omega)}^2, \quad \forall u_h \in \mathcal{V}_h^{\text{ag}},$$

It is also important to note that, by construction, $\mathcal{V}_h^{\text{ag}}(U)$ for $U \in \mathcal{T}_h^{\text{ag}}$ is a subspace of $\mathcal{P}_p(U)$ (for simplices) of $\mathcal{Q}_p(U)$ for hexahedra, solving the issues in the $\gamma \rightarrow \infty$ limit of F-GP and B-GP. As a result, the method preserves the convergence properties of $\mathcal{V}_h^{\text{act}}$. We summarise these observations in the following definition.

Definition 5.1. Let $0 \leq s \leq n \leq m$, where m is the order of $\mathcal{V}_h^{\text{in}}$. A suitable discrete extension operator $\mathcal{E}_h^{\text{ag}} : \mathcal{V}_h^{\text{in}} \rightarrow \mathcal{V}_h^{\text{act}}$ must satisfy the following properties:

(i) *Continuity:*

$$\|\mathcal{E}_h^{\text{ag}}(v_h)\|_{L^2(\Omega_h^{\text{act}})} \lesssim \|v_h\|_{L^2(\Omega_h^{\text{in}})}, \quad \|\nabla \mathcal{E}_h^{\text{ag}}(v_h)\|_{L^2(\Omega_h^{\text{act}})} \lesssim \|\nabla v_h\|_{L^2(\Omega_h^{\text{in}})}, \quad \forall v_h \in \mathcal{V}_h^{\text{in}}. \quad (18)$$

(ii) *Approximability:*

$$\inf_{v_h \in \mathcal{V}_h^{\text{in}}} \|u - \mathcal{E}_h^{\text{ag}}(v_h)\|_{H^s(\Omega)} \lesssim h^{n-s+1} \|u\|_{H^{n+1}(\Omega)}, \quad \forall u \in H^{n+1}(\Omega). \quad (19)$$

The image $\mathcal{V}_h^{\text{ag}} \doteq \text{Im}(\mathcal{E}_h^{\text{ag}}) \subset \mathcal{V}_h^{\text{act}}$ is a suitable AgFE space.

Proposition 5.2. Let $\mathcal{E}_h^{\text{ag}}$ satisfy Def. 5.1. Let $\mathcal{V}_h^{\text{ag}}(h) \doteq H^2(\Omega) + \mathcal{V}_h^{\text{ag}}$, endowed with the norm

$$\|v\|_{\mathcal{V}_h^{\text{ag}}(h)}^2 \doteq \|\nabla v\|_{L^2(\Omega)}^2 + \|\tau^{\frac{1}{2}} v\|_{L^2(\Gamma_D)}^2 + \sum_{T \in \mathcal{T}_h^{\text{act}}} h_T^2 \|v\|_{H^2(T)}^2, \quad \forall v \in \mathcal{V}_h^{\text{ag}}(h).$$

³One could consider alternative expressions for the constraints. E.g., one could skip the aggregate owner map $O_h^{\text{dof} \rightarrow \text{ag}}$ and simply compute an average of the constraints from all aggregates that contain the ill-posed DOF. However, this choice would have a very negative impact on the sparsity pattern of the resulting linear system and was originally discarded.

It holds:

$$a_h(u_h, u_h) \gtrsim \|u_h\|_{\mathcal{V}_h^{\text{ag}}(h)}^2, \quad a_h(u, v_h) \lesssim \|u\|_{\mathcal{V}_h^{\text{ag}}(h)} \|v_h\|_{\mathcal{V}_h^{\text{ag}}(h)}, \quad (20)$$

for any $u_h, v_h \in \mathcal{V}_h^{\text{ag}}$, $u \in \mathcal{V}_h^{\text{ag}}(h)$. Thus, there is a unique

$$u_h \in \mathcal{V}_h^{\text{ag}} : a_h(u_h, v_h) = b(v_h), \quad \forall v_h \in \mathcal{V}_h^{\text{ag}}. \quad (21)$$

Furthermore, the condition number κ of the resulting linear system when using a standard Lagrangian basis for $\mathcal{V}_h^{\text{in}}$ holds $\kappa \lesssim h^{-2}$.

Proof. In order to prove (20), the Nitsche terms can readily be bounded as in Prop. 4.2 using (18). The condition number proof follows the same lines as the one for the GP in Prop. 4.2 (see [16]). \square

Proposition 5.3. *Let m be the order of $\mathcal{V}_h^{\text{act}}$. If $u \in H^{m+1}(\Omega)$, $m \geq n \geq 1$, is the solution of (3) or (4) and $u_h \in \mathcal{V}_h^{\text{ag}}$ is the solution of (21), then:*

$$\|u - u_h\|_{\mathcal{V}(h)} \lesssim h^n |u|_{H^{m+1}(\Omega)}, \quad \|u - u_h\|_{L^2(\Omega)} \lesssim h^{n+1} |u|_{H^{m+1}(\Omega)}.$$

Proof. The convergence analysis is standard and relies on the approximability property (19). \square

Proposition 5.4. *The discrete extension operator $\mathcal{E}_h^{\text{ag}}$ constructed with expression (17) satisfies the conditions in Def. 5.1.*

Proof. The continuity in (18) relies on the fact that the constrained DOF values in (17) can be bounded by interior DOFs under the assumption that the aggregate sizes are proportional to the root cell size. The complete proof can be found in [16, Corollary 5.3] for a general AgFE space, which can be either $\mathcal{V}_h^{\text{in}}$ or the discontinuous FE space of its gradients. The proof of the approximability property (19) can be found in [16, Lemma 5.10]. \square

5.1. Ghost penalty with discrete extension. In this section, we propose a novel scheme, which combines the discrete extension operator defined above for the AgFEM and the GP stabilisation ideas. This development is motivated by the *locking* phenomenon of GP methods as $\gamma \rightarrow \infty$. The idea is to penalise the distance between the solution in the (unconstrained) $\mathcal{V}_h^{\text{act}}$ space and the one in $\mathcal{V}_h^{\text{ag}}$.

In Section 5, we have defined the discrete extension operator $\mathcal{E}_h^{\text{ag}} : \mathcal{V}_h^{\text{in}} \rightarrow \mathcal{V}_h^{\text{ag}}$. Let us define the projector $\mathcal{P}_h^{\text{ag}} : \mathcal{V}_h^{\text{act}} \rightarrow \mathcal{V}_h^{\text{ag}}$ that takes $v_h \in \mathcal{V}_h^{\text{act}}$, computes its restriction to the interior $v_h|_{\Omega_h^{\text{in}}} \in \mathcal{V}_h^{\text{in}}$ and applies the extension $\mathcal{E}_h^{\text{ag}}$, i.e., $\mathcal{P}_h^{\text{ag}}(v_h) \doteq \mathcal{E}_h^{\text{ag}}(v_h|_{\Omega_h^{\text{in}}})$. Next, we define the following stabilisation term:

$$s_h(u_h, v_h) \doteq \sum_{U \in \mathcal{T}_h^{\text{ag}}} \left(\gamma h_U^{-2} \left(u_h - \mathcal{P}_h^{\text{ag}}(u_h) \right), v_h - \mathcal{P}_h^{\text{ag}}(v_h) \right)_{U^*}, \quad (22)$$

where U^* can be chosen to be U or $U \setminus \Omega$ (i.e., only adding stability in the exterior part). We refer to method (22) as **weak AgFEM by L^2 product (W-Ag- L^2)**. We note that this term can be computed cell-wise, in the spirit of so-called local projection stabilisation methods [46, 47]. On the other hand, the term vanishes at the root cell of the aggregate by construction, i.e., it is only active on Ω_h^{cut} . Alternatively, one could consider an L^2 -projection at each aggregate U , as in the B-GP. It is also obvious to check that this method converges to the AgFEM in the limit $\gamma \rightarrow \infty$. Alternatively, we can consider a stabilisation that relies on the H^1 product:

$$s_h(u_h, v_h) \doteq \sum_{U \in \mathcal{T}_h^{\text{ag}}} \left(\gamma \nabla \left(u_h - \mathcal{P}_h^{\text{ag}}(u_h) \right), \nabla \left(v_h - \mathcal{P}_h^{\text{ag}}(v_h) \right) \right)_{U^*}, \quad (23)$$

that is, a **weak AgFEM by H^1 product (W-Ag- ∇)**, where again U^* can be U or $U \setminus \Omega$. Its implementation is as easy as the previous one, but does not require to compute a characteristic mesh size h_U .

Proposition 5.5. *The expressions of s_h in (22) and (23) are suitable GP stabilisation that satisfies the conditions (7)-(9) in Def. 4.1.*

Proof. Let us start proving the extended stability (7) as follows. Using the stability of the discrete extension operator (18) and the triangle inequality, we get:

$$\begin{aligned} \|\nabla u_h\|_{L^2(\Omega_h^{\text{act}})}^2 &\leq \|\nabla u_h\|_{L^2(\Omega)}^2 + \|\nabla u_h - \nabla \mathcal{P}_h^{\text{ag}}(u_h)\|_{L^2(\Omega_h^{\text{cut}} \setminus \Omega)}^2 + \|\nabla \mathcal{P}_h^{\text{ag}}(u_h)\|_{L^2(\Omega_h^{\text{cut}} \setminus \Omega)}^2 \\ &\leq \|\nabla u_h - \nabla \mathcal{P}_h^{\text{ag}}(u_h)\|_{L^2(\Omega_h^{\text{cut}} \setminus \Omega)}^2 + C \|\nabla u_h\|_{L^2(\Omega_h^{\text{in}})}^2, \end{aligned} \quad (24)$$

for any $u_h \in \mathcal{V}_h^{\text{act}}$. The result for s_h in (22) can be obtained by bounding the second term in (24) using the quasi-uniformity of the background mesh $\mathcal{T}_h^{\text{act}}$, the standard inverse inequality in $\mathcal{T}_h^{\text{act}}$ and the assumption that aggregate size h_U is proportional to the root cell size times a constant that does not depend on h .

For weak consistency, we need to extend the definition of s_h for $u \in H^{n+1}(\Omega_h^{\text{act}})$. To this end, we invoke the standard Scott-Zhang interpolant $\pi_h^{\text{sz}} : H^{n+1}(\Omega_h^{\text{act}}) \rightarrow \mathcal{V}_h^{\text{act}}$, using the definition in [48]. We let $\tilde{\mathcal{P}}_h^{\text{ag}} = \mathcal{P}_h^{\text{ag}} \circ \pi_h^{\text{sz}}$; obviously $\tilde{\mathcal{P}}_h^{\text{ag}}(u_h) = \mathcal{P}_h^{\text{ag}}(u_h)$, if $u_h \in \mathcal{V}_h^{\text{act}}$, since π_h^{sz} is a projection. Hence, weak consistency (9) of the proposed methods can readily be proved using the optimal approximation properties of $\mathcal{V}_h^{\text{ag}}$ in (19).⁴

$$|s_h(\mathcal{E}^{n+1}(u), v_h)| \lesssim |\mathcal{E}^{n+1}(u) - \tilde{\mathcal{P}}_h^{\text{ag}}(\mathcal{E}^{n+1}(u))|_{H^1(\Omega_h^{\text{act}})} \|\nabla v_h\|_{L^2(\Omega_h^{\text{act}})} \lesssim h^n |u|_{H^{n+1}(\Omega)} \|v_h\|_V(h),$$

for s_h in (23) and

$$|s_h(\mathcal{E}^{n+1}(u), v_h)| \lesssim \sum_{U \in \mathcal{T}_h^{\text{ag}}} h^{-2} \|\mathcal{E}^{n+1}(u) - \tilde{\mathcal{P}}_h^{\text{ag}}(\mathcal{E}^{n+1}(u))\|_{L^2(U)}^2 \|v_h\|_{L^2(U)} \lesssim h^n |u|_{H^{n+1}(\Omega)} \|v_h\|_V(h)$$

for s_h in (22). The proof of continuity (8) relies on the H^1 -stability of the Scott-Zhang interpolant and the discrete extension operator in (18). \square

We observe that, for $U^* \doteq U \setminus \Omega$, W-Ag- ∇ in (23) can also be understood as an improvement of the so-called finite cell method [49] that is both convergent and robust. Instead of subtracting a projection, the finite cell method adds a grad-grad term on $\Omega_h^{\text{act}} \setminus \Omega$, premultiplied by a numerical parameter. When the parameter is large, convergence is deteriorated. When the parameter is small, robustness is affected. Subtracting the projection, these problems are solved, since the resulting method enjoys weak consistency.

6. IMPLEMENTATION ASPECTS

The implementation of the previous methods have some non-standard requirements that are not present in body-fitted FE codes. First, there are some geometrical functions that have to be implemented.

All methods, but the F-GP (15), require the computation of an aggregated mesh with the properties described in Sec. 2. Furthermore, all the GP methods, but the original bulk penalty in (14), require the n -face to aggregate map described in Sec. 5. Besides, the GP method needs to identify the set of faces that are in touch with cut cells and intersect the domain Ω . In any case, the implementation of all these steps is quite straightforward and can be easily implemented in distributed memory machines (see [37, 38]).

The implementation of F-GP involves jumps of normal derivatives up to the order of the FE space. This functionality is uncommon in FE software (see, e.g., [50, 51, 52]). The implementation of the B-GP methods requires the computation of aggregate-wise L^2 projections, which is a non-obvious task in FE software, since it breaks the standard procedure, namely to compute cell-local matrices, assemble the local matrices in a global sparse array and solve a global linear system.

In order to avoid this implementation issue, we can consider an interpolator in the spirit of W-Ag- L^2 . We replace the aggregate-wise L^2 projection in (14) by the interpolation of the FE function on the root cell over the aggregate. Let $\mathcal{V}_h^{\#, -}$ be the DG counterpart of $\mathcal{V}_h^\#$, for $\# \in \{\text{in}, \text{cut}\}$. We can define the DG discrete extension operator $\mathcal{E}_h^{\text{ag}, -}$ using the definition above for the DG spaces. We note that the construction of the extension is much simpler in this case, since all DOFs belong to cells. Since $\mathcal{V}_h^{\text{in}} \subset \mathcal{V}_h^{\text{in}, -}$, we readily obtain $\mathcal{E}_h^{\text{ag}, -} : \mathcal{V}_h^{\text{in}} \rightarrow \mathcal{V}_h^{\text{act}, -}$. Analogously, we can define the projector $\mathcal{P}_h^{\text{ag}, -} : \mathcal{V}_h^{\text{act}} \rightarrow \mathcal{V}_h^{\text{ag}, -}$ that takes $v_h \in \mathcal{V}_h^{\text{act}}$, computes its restriction to the interior $v_h|_{\Omega_h^{\text{in}}} \in \mathcal{V}_h^{\text{in}}$ and applies the DG extension

⁴We note that AgFEM does not require to define an extension of the continuous solution and the approximability property is only needed in Ω . In any case, the proof in [16, Lemma 5.10] also applies for Ω_h^{act} .

$\mathcal{E}_h^{\text{ag},-}$, i.e., $\mathcal{P}_h^{\text{ag},-}(v_h) \doteq \mathcal{E}_h^{\text{ag},-}(v_h|_{\Omega_h^{\text{in}}})$. Now, we can define an alternative **B-GP stabilisation with interpolation (B-GP-i)** as follows:

$$s_h(u_h, v_h) \doteq \sum_{U \in \mathcal{T}_h^{\text{ag}}} \left(\gamma h_U^{-2} \left(u_h - \mathcal{P}_h^{\text{ag},-}(u_h) \right), v_h - \mathcal{P}_h^{\text{ag},-}(v_h) \right)_U. \quad (25)$$

The proof for the bulk penalty method (14) readily applies for this version, since the aggregate-wise interpolant share the required continuity and error bounds of the aggregate-wise L^2 projection. On the other hand, it is penalising the component that does not belong to the same space, thus it has the same locking problems. Since the interpolant-based version simplifies the implementation, this is the one to be used in Sect. 7.

The GP and AgFE methods make use of an ill-posed to well-posed DOF that can be readily computed with the geometrical machinery described above and the local-to-global DOF map. These methods require the implementation of a discrete extension operator. In general, it can be stored as the set of linear constraints in (17) that can be implemented cell-wise (traversing all root cells). The computation of this constraints is much simpler than in h and hp -adaptivity (see, e.g., [50, 51, 53]). It requires to evaluate the shape functions of the root cell in the nodes of the ill-posed DOFs (see (17)). In most FE codes, it requires the implementation of the geometrical map inverse, in order to map points from the physical to the reference space, which is not standard in general. This problem is trivial for Cartesian background meshes, which is arguably the most natural and efficient choice.

For the (strong) AgFEM, one must impose these constraints in the assembly process. This is readily available (for more complex constraints) in any code that allows adaptive mesh refinement with hanging nodes (see, e.g., [50]). For the novel weak versions W-Ag- L^2 and W-Ag- ∇ , the assembly process does not involve the imposition of constraints. However, the local matrix in cut cells does not only include the local DOFs but also the local DOFs of the root cell. E.g., for W-Ag- ∇ , we have to assemble the following entries:

$$\begin{aligned} (\nabla \phi_i, \nabla \phi_j)_T, & \quad i, j \in \overline{\mathcal{O}}_h^{\text{nf} \rightarrow \text{dof}}(T), \\ \left(\nabla \phi_i, \mathcal{E}_h^{\text{ag}}(\nabla \phi_k) \right)_T, & \quad i \in \overline{\mathcal{O}}_h^{\text{nf} \rightarrow \text{dof}}(T), k \in \mathcal{O}_h^{\text{ipd} \rightarrow \text{wpd}} \circ \overline{\mathcal{O}}_h^{\text{nf} \rightarrow \text{dof}}(T), \end{aligned}$$

and the transpose of the second term, for any $T \in \mathcal{T}_h^{\text{cut}}$.

7. NUMERICAL EXPERIMENTS

7.1. Methods and parameter space. We collect in Table 1 all the numerical methods that will be analysed in this work, in terms of the stabilisation term s_h and the FE space being used. We consider first the F-GP method defined in (15). We include the expression of s_h for linear elements. Higher order approximations would require to evaluate inter-facet jumps of higher order derivatives that are not available in the numerical framework Gridap [52]. We also consider the modification of this method (16), that only penalises intra-aggregate facets (A-GP). As indicated in Sect. 6, we consider the interpolation-based B-GP-i method (25). We also analyse the results for both versions of the weak AgFEM: W-Ag- L^2 and W-Ag- ∇ , i.e., using the L^2 product (22) and H^1 product (23). In both cases, we set $U^* = U$. All these methods make use of the standard FE space $\mathcal{V}_h^{\text{act}}$ on the active mesh $\mathcal{T}_h^{\text{act}}$. Finally, we compare all these stabilised formulations against the **strong version of AgFEM (S-Ag)** in Sect. 5, which makes use of the FE space $\mathcal{V}_h^{\text{ag}}$.

We show in Table 2 the parameter space being explored. We have reduced, as much as possible, this space, due to length constraints. We solve the Poisson problem (3) and linear elasticity (4) discrete problems for two different sets of boundary conditions, namely weak imposition of Dirichlet boundary conditions on the whole boundary and Neumann and strong Dirichlet boundary conditions. This way, we can analyse the behaviour of the methods with respect to Nitsche terms and Neumann boundary conditions separately. To compute errors analytically, we use polynomial manufactured solutions of the form $u(x, y) = (x + y)^{m+1}$ in 2D and $u(x, y, z) = (x + y + z)^{m+1}$ in 3D, with m the order of the FE space.

We have observed that the use of simplicial and hexahedral meshes leads to similar conclusions. So, we only show results for simplicial meshes below. We have considered the square in 2D and the cube, a tilted cube, the sphere and the 8-norm sphere in 3D. All geometries are represented in Figure 2. They are centred







Acronym	Stabilisation form $s_h(u_h, v_h)$	FE space	Legend
F-GP	$\sum_{F \in \mathcal{F}_h^{\text{gh, cut}}} (\gamma h_F \llbracket \partial_n u_h \rrbracket, \llbracket \partial_n v_h \rrbracket)_F$	$\mathcal{V}_h^{\text{act}}$	
A-GP	$\sum_{F \in \mathcal{F}_h^{\text{gh, ag}}} (\gamma h_F \llbracket \partial_n u_h \rrbracket, \llbracket \partial_n v_h \rrbracket)_F$	$\mathcal{V}_h^{\text{act}}$	
B-GP-i	$\sum_{U \in \mathcal{T}_h^{\text{ag}}} \left(\gamma h_U^{-2} \left(u_h - \mathcal{P}_h^{\text{ag, -}}(u_h) \right), v_h - \mathcal{P}_h^{\text{ag, -}}(v_h) \right)_U$	$\mathcal{V}_h^{\text{act}}$	
W-Ag- L^2	$\sum_{U \in \mathcal{T}_h^{\text{ag}}} \left(\gamma h_U^{-2} \left(u_h - \mathcal{P}_h^{\text{ag}}(u_h) \right), v_h - \mathcal{P}_h^{\text{ag}}(v_h) \right)_U$	$\mathcal{V}_h^{\text{act}}$	
W-Ag- ∇	$\sum_{U \in \mathcal{T}_h^{\text{ag}}} \left(\gamma \nabla \left(u_h - \mathcal{P}_h^{\text{ag}}(u_h) \right), \nabla \left(v_h - \mathcal{P}_h^{\text{ag}}(v_h) \right) \right)_U$	$\mathcal{V}_h^{\text{act}}$	
S-Ag	0	$\mathcal{V}_h^{\text{ag}}$	

TABLE 1. Summary of the different methods used and their corresponding symbols in the numerical examples.

Description	Considered methods/values
Model problem	Poisson equation (Nitsche's formulation); Linear elasticity (Neumann and strong Dirichlet)
Analytical solution	$u(x, y) = (x + y)^{m+1}$ (2D) and $u(x, y, z) = (x + y + z)^{m+1}$ (3D) m is the FE interpolation order
Problem geometry	2D: square; 3D: cube, tilted cube, sphere, 8-norm sphere
Interpolation	C^0 linear and quadratic FEs on simplicial meshes
Coef. in Nitsche's penalty term	$\beta = 10.0 m^2$

TABLE 2. Summary of the main parameters and computational strategies used in the numerical examples.

at the origin of coordinates. For weak Dirichlet tests, we simulate the whole geometry; while only the region in the first quadrant/octant for mixed boundary conditions. We have configured all geometries, in a similar way as in [54], to ensure that the small cut cell problem is present in all cases with $\min_{T \in \mathcal{T}_h^{\text{act}}} \eta_T$ of the order of 10^{-8} . In the case of the square, cube and 8-norm sphere, we also enforce sliver cuts. We have considered both linear and quadratic C^0 Lagrangian FE spaces. We pay particular attention to the penalty parameter γ ; as we will see, some methods are highly sensitive to this value.

7.2. Experimental environment. All the algorithms have been implemented in the Gridap open-source scientific software project [52]. Gridap is a novel framework for the implementation of grid-based algorithms for the discretisation of PDEs written in the Julia programming language. Gridap has a user interface that resembles the whiteboard mathematical statement of the problem. The framework leverages the Julia just-in-time (JIT) compiler to generate high-performant code. Gridap is extensible and modular and has many available plugins. In particular, we have extensively used and extended the GridapEmbedded plugin, which provides all the mesh queries required in the implementation of the embedded methods under consideration, level set surface descriptions and constructive solid geometry. We use the cond() method provided by Julia to compute condition numbers. Condition numbers have been computed in the 1-norm for efficiency reasons. It was not possible to compute the 2-norm condition number for all cases with the available computational resources.

The numerical experiments have been carried out at the TITANI cluster of the Universitat Politècnica de Catalunya (Barcelona, Spain), and NCI-Gadi [55], hosted by the Australian National Computational Infrastructure Agency (NCI). NCI-Gadi is a petascale machine with 3024 nodes, each containing 2x 24-core Intel Xeon Scalable *Cascade Lake* processors and 192 GB of RAM. All nodes are interconnected via Mellanox Technologies' latest generation HDR InfiniBand technology.

7.3. Sensitivity analysis. We consider first log-log plots. They show values of the penalty parameter $\gamma = 10^{-\alpha}$ for $\alpha \in \{-2, -1, 0, 1, 2, 4, 6, 8\}$, in the X-axis, and the value of the condition number (in 1-norm)

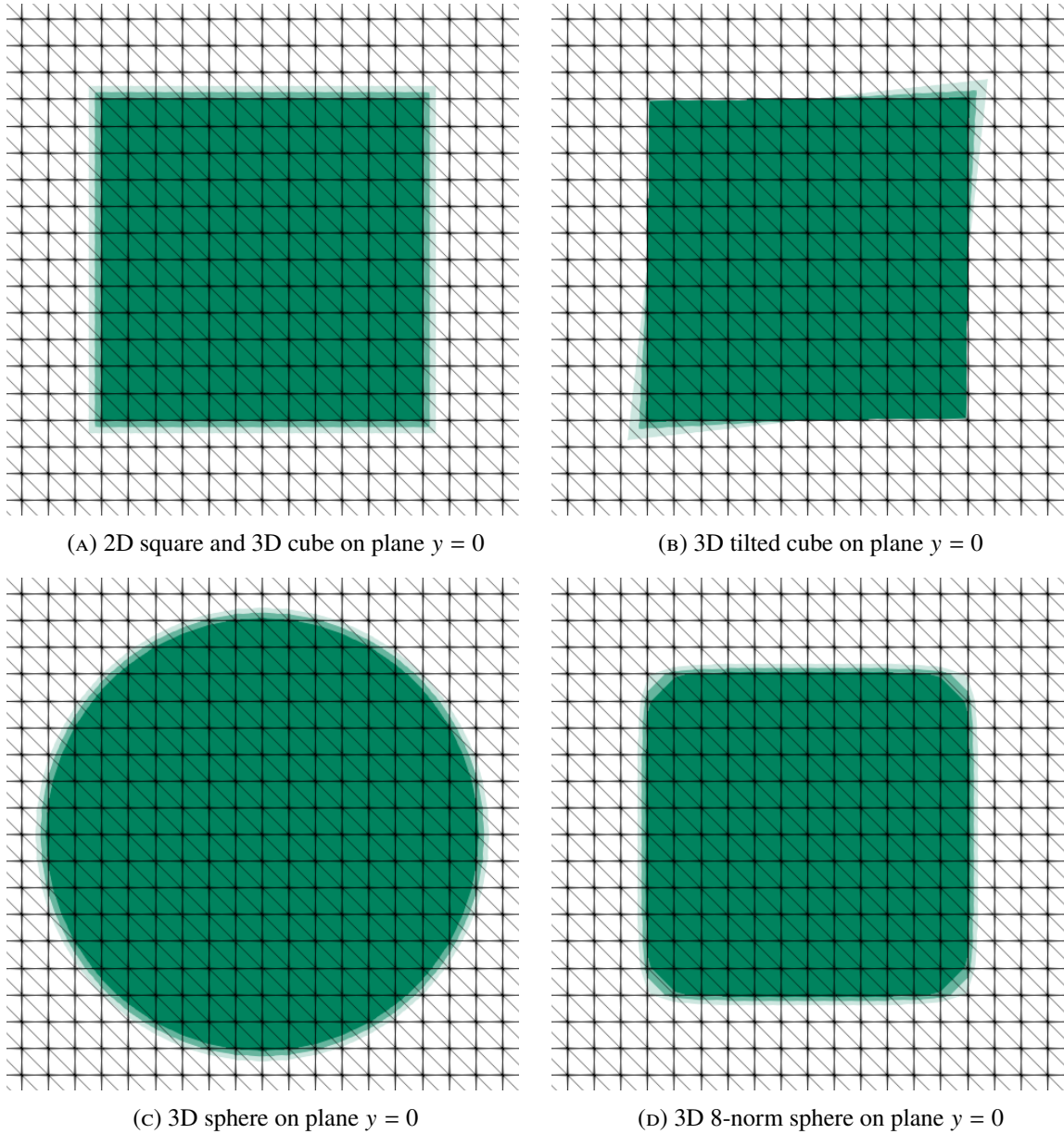


FIGURE 2. Geometries considered in the sensitivity analysis. We superpose different configurations of each geometry, with increasing opacity, to expose how we have shrunk the geometries to force cut volumes of the order of 10^{-8} . We refer the reader to [54] for the level set descriptions of 2a, 2b and 2d.

and the L^2 and H^1 errors, in the Y-axis. These plots allow us to easily compare the behaviour of the different methods and observe their dependency with respect to the penalty parameter γ .

7.3.1. 2D results. We show in Figure 3 the plots corresponding to the 2D square using both linear and quadratic FEs for the solution of the Poisson problem with weak imposition of Dirichlet boundary conditions.

Let us consider first the condition number plots. For linear elements, we observe that all weak methods have the same behaviour. In all cases, the minimum is attained at $\gamma = 1$. The condition number increases as $\gamma \rightarrow 0$. The stabilisation is not enough to fix the small cut cell problem effect on the condition number. The condition number linearly increases as $\gamma \rightarrow \infty$. This phenomenon is well-understood. The minimum eigenvalue does not grow with γ , since eigenvectors can be in the kernel of the penalty term, i.e., they can belong to a subspace that cancels the penalty term. On the contrary, the maximum eigenvalue linearly increases with γ . The results for second order elements are similar, even though there is a more erratic

behaviour for values of γ below 1. The condition number of the strong AgFEM (S-Ag) is constant (the method does not depend on γ) and is below weak schemes in all cases.

Now, we analyse the L^2 and H^1 error of the methods. For linear elements, we can observe the *locking* phenomenon predicted in Sect. 4.3 in the limit $\gamma \rightarrow \infty$. We can observe that we have three types of weak methods. The worst method is F-GP, because it is the one that rigidises on all ghost skeleton facets (see Sect. 4.3). The methods that only introduce intra-aggregate rigidisation, i.e., the weaker facet-stabilisation A-GP and the bulk-based method B-GP-i, show slightly lower errors, but still exhibit *locking* and are not convergent methods in the limit. It is more serious for practical purposes the strong sensitivity of these methods to γ . The behavior is highly erratic. For linear elements, the best result is for $\gamma = 10^{-2}$, but this is not the case for quadratic elements. Besides, F-GP, A-GP and B-GP-i are worse than W-Ag- L^2 , W-Ag- ∇ and S-Ag in all cases but $\gamma = 1$, where B-GP-i has a similar behavior as the Ag-based methods. The novel weak versions of AgFEM are far less sensitive to γ . The methods can exhibit some instability as $\gamma \rightarrow 0$, since the stabilisation is not enough. However, the methods are very robust for $\gamma \geq 1$. On the other hand, as stated in Sect. 5.1, W-Ag-* show the same error as S-Ag, indicating that these algorithms do converge to S-Ag in the limit $\gamma \rightarrow \infty$. Thus, these methods are not affected by any *locking* in this limit.

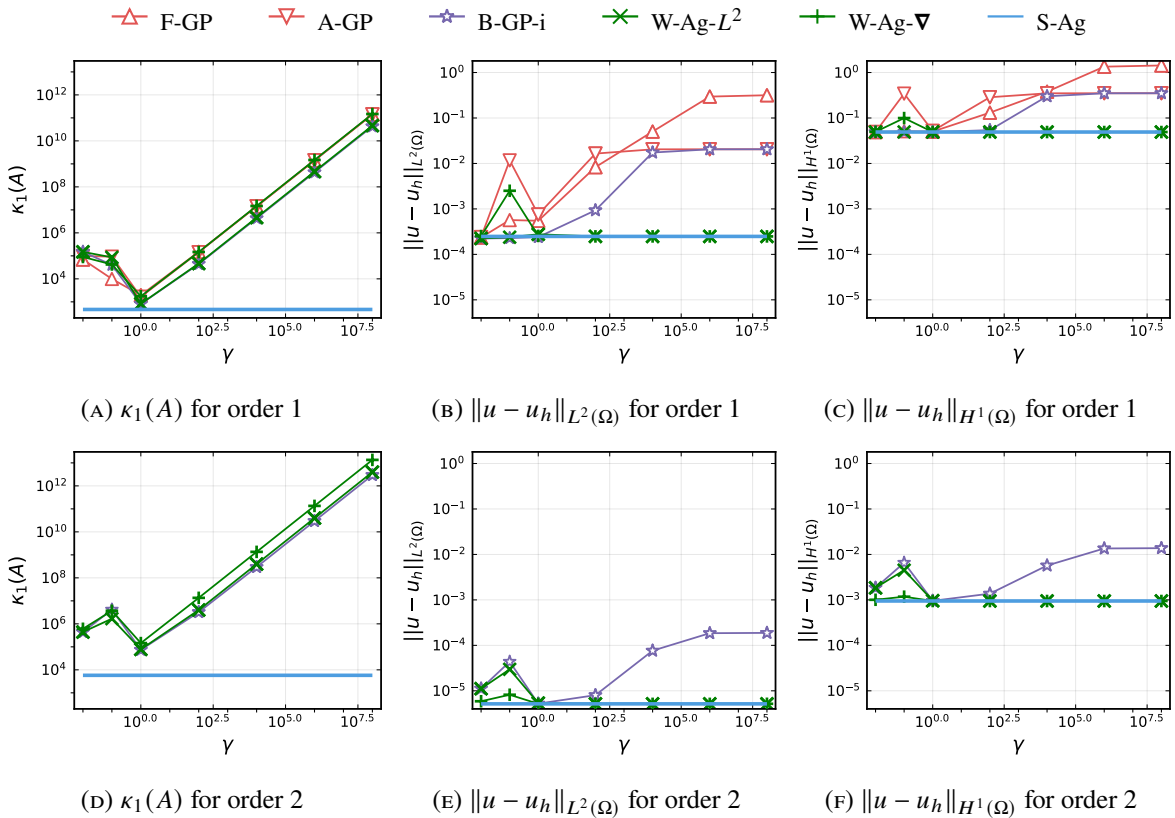


FIGURE 3. Condition number $\kappa_1(A)$, and error norms $\|u - u_h\|_{L^2(\Omega)}$ and $\|u - u_h\|_{H^1(\Omega)}$ vs. penalty parameter γ for the Poisson problem with Nitsche's method on the square using linear and quadratic elements in a 40×40 structured triangular mesh.

Before reporting the 3D results, we take a closer look at the *locking* phenomenon. In Figure 4, we consider plots of the solution in the square for $\gamma = 10000$, using linear elements in a 20×20 structured triangular mesh. As expected, the F-GP solution is affected by severe locking and completely wrong. The A-GP and B-GP-i solutions are barely indistinguishable; they are still polluted by locking, which constraints the values of interior DOFs away from the analytical solution. Finally, W-Ag-* are completely free of locking and coincide with the S-Ag solution.

7.3.2. 3D results. We show in Figure 5 the same kind of plots for 3D geometries. In this test, we consider three different geometries, in order to evaluate whether the geometry affects the behavior of the different methods. We have considered the cube, a tilted cube and a sphere. We consider linear elements, only. We

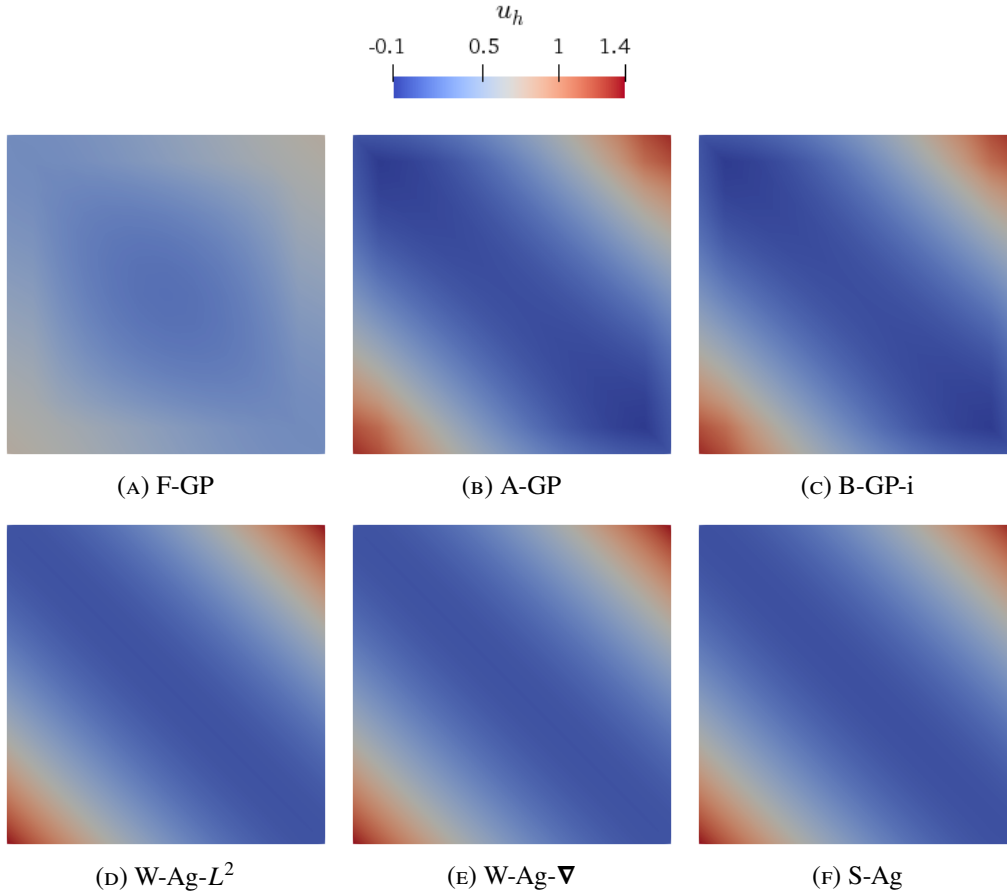


FIGURE 4. Solution of the Poisson problem with Nitsche's method on the square, using linear elements in a 20×20 structured triangular mesh. All *weak* methods take $\gamma = 10000$.

observe essentially the same behavior as in 2D. The results for all methods are quite insensitive to the geometry. The sphere is an *easier* geometry in general, since it is smoother and does not involve corners. However, the results are very similar to the ones for the cube and tilted cube. The only difference would be the slightly better results of weak methods for γ below 1. Anyway, the more important observations clearly apply. F-GP, A-GP and B-GP-i are very sensitive to γ and exhibit *locking*. W-Ag-* methods are very insensitive to γ . The S-Ag method is close to the optimal value in most situations, while parameter-free.

We compare now the linear elasticity problem and Neumann boundary conditions and consider both linear and quadratic elements on the 3D cube. In this case, W-Ag-* errors are totally independent of γ , also for low values of γ . Condition number plots have the same behavior as above; for the largest values of γ the problem is so ill-conditioned that the solution is severely affected by rounding errors, but such a value of γ is for presentation purposes and certainly not a value to be used in practise. The W-GP, A-GP and B-GP-i methods show the same problems discussed above. S-Ag exhibits optimal condition numbers and errors in all cases. The results are very similar for linear and quadratic FEs. The only difference is that the condition number of S-Ag is about one order of magnitude lower than the weak methods.

In Figure 7, we analyse the behavior of the methods for linear elasticity and Neumann boundary conditions on the sphere for both linear and quadratic FEs. Again, W-Ag-* methods turn to be very insensitive to γ . F-GP, A-GP and B-GP-i show the same bad behavior indicated in the previous examples. The main difference with respect to above is the fact that the condition number of S-Ag for quadratic elements is about one order of magnitude larger than the minimum value obtained with weak schemes.

7.4. Results under refinement. In this section, we analyse results in a more standard way. We consider the variation of the condition number and L^2 and H^1 errors as we refine the mesh. We show the results for three different values, $\gamma \in \{1, 100, 10^8\}$. In Figure 8, we consider the Poisson problem with Nitsche's method for linear elements on the cube. For the condition number bounds, we observe that the weak

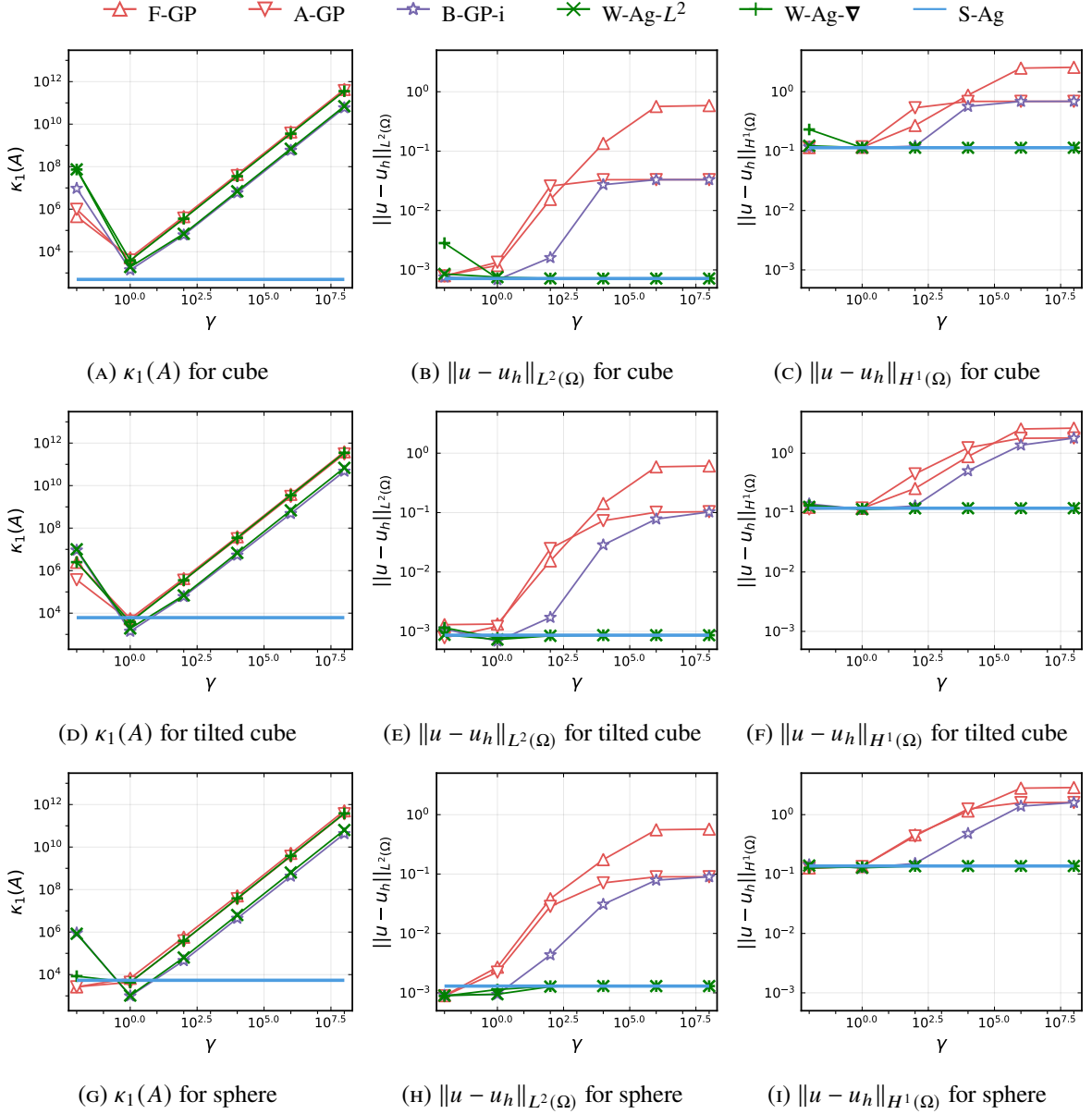


FIGURE 5. Condition number $\kappa_1(A)$, and error norms $\|u - u_h\|_{L^2(\Omega)}$ and $\|u - u_h\|_{H^1(\Omega)}$ vs. penalty parameter γ for the Poisson problem with Nitsche's method on the cube, tilted cube and sphere, for order 1 in a $40 \times 40 \times 40$ structured tetrahedral mesh.

methods are in some cases still in a pre-asymptotic regime and in all cases above S-Ag. The loss of convergence of F-GP with increasing values of γ is very clear. As indicated above, the results for A-GP and B-GP-i are slightly better, but they still show the loss of convergence in this limit. W-Ag-* and S-Ag practically show the same convergence behaviour in all cases. We show in Figure 9 the same plots for elasticity, Neumann boundary conditions and the 8-norm sphere using quadratic elements. Despite all the differences in the numerical setup, the results are strikingly similar and the same conclusions apply.

8. CONCLUSIONS

In this work, we have analysed the link between *weak* ghost penalty methods, which rely on a stabilisation term, and *strong* AgFEMs, which rely on discrete extension operators for the definition of the FE spaces. When comparing these two families of methods, we observe that standard GP formulations, e.g., the one being used in the CutFEM method, do not lead to acceptable strong versions. The problem is that the kernel of the penalty term does not enjoy the right approximability properties. The stabilisation is rigidising too much the solution, and exhibits a *locking* phenomenon as the penalty parameter increases.

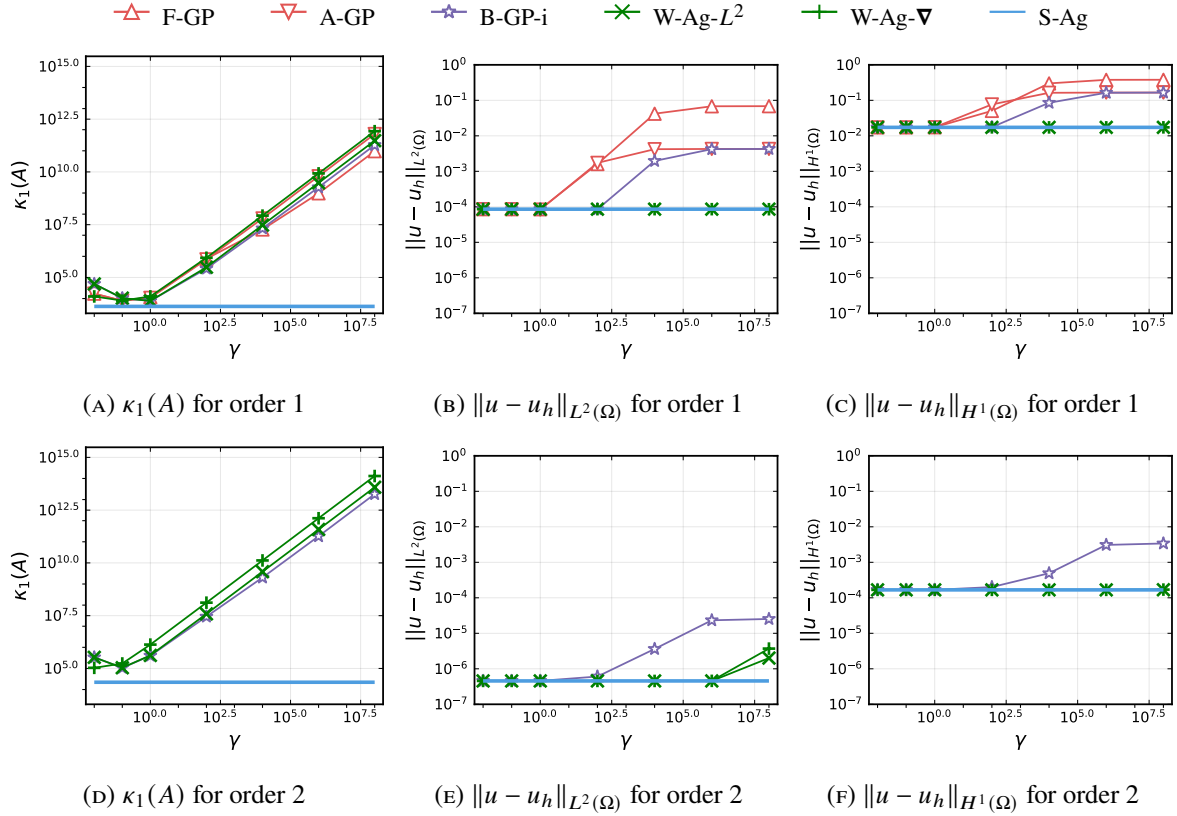


FIGURE 6. Condition number $\kappa_1(A)$, and error norms $\|u - u_h\|_{L^2(\Omega)}$ and $\|u - u_h\|_{H^1(\Omega)}$ vs. penalty parameter γ for the linear elasticity problem with Neumann and strong Dirichlet boundary conditions on the cube using linear and quadratic elements in a $40 \times 40 \times 40$ structured tetrahedral mesh.

As a result, we propose novel GP methods that explicitly use the discrete extension operator in AgFEM. The idea is to penalise the distance between the standard FE space and the AgFE space. The penalty term has a local stabilisation structure in which the distance between these two spaces is expressed in terms of the difference between the solution and the discrete extension of its value on interior cells. The kernel of the penalty term is the AgFE space. Thus, these methods converge to the strong AgFEM as the penalty parameters increases and are *locking-free*.

We have carried out a thorough numerical analysis, in which we have compared all the methods with respect to condition number, L^2 and H^1 error. We have considered linear and quadratic FEs, Poisson and linear elasticity problems, weak imposition of Dirichlet conditions using Nitsche's method and Neumann boundary conditions, and a set of geometries in 2D and 3D. Due to the problems commented above, standard GP formulations are strongly sensitive to the penalty parameter, losing convergence properties for moderate to large values of this parameter. On the contrary, the new GP methods that are weak versions of AgFEM are much less sensitive to the penalty parameter and their convergence is preserved in all cases. They are a good alternative to the strong formulation of AgFEM and are systematically superior to existing GP formulations.

ACKNOWLEDGMENTS

This research was partially funded by the Australian Government through the Australian Research Council (project number DP210103092), the European Commission under the FET-HPC ExaQute project (Grant agreement ID: 800898) within the Horizon 2020 Framework Programme and the project RTI2018-096898-B-I00 from the "FEDER/Ministerio de Ciencia e Innovaci3n – Agencia Estatal de Investigaci3n". F. Verdugo acknowledges support from the Spanish Ministry of Economy and Competitiveness through the "Severo Ochoa Programme for Centers of Excellence in R&D (CEX2018-000797-S)". F. Verdugo acknowledges support from the *Secretaria d'Universitats i Recerca* of the Catalan Government in the

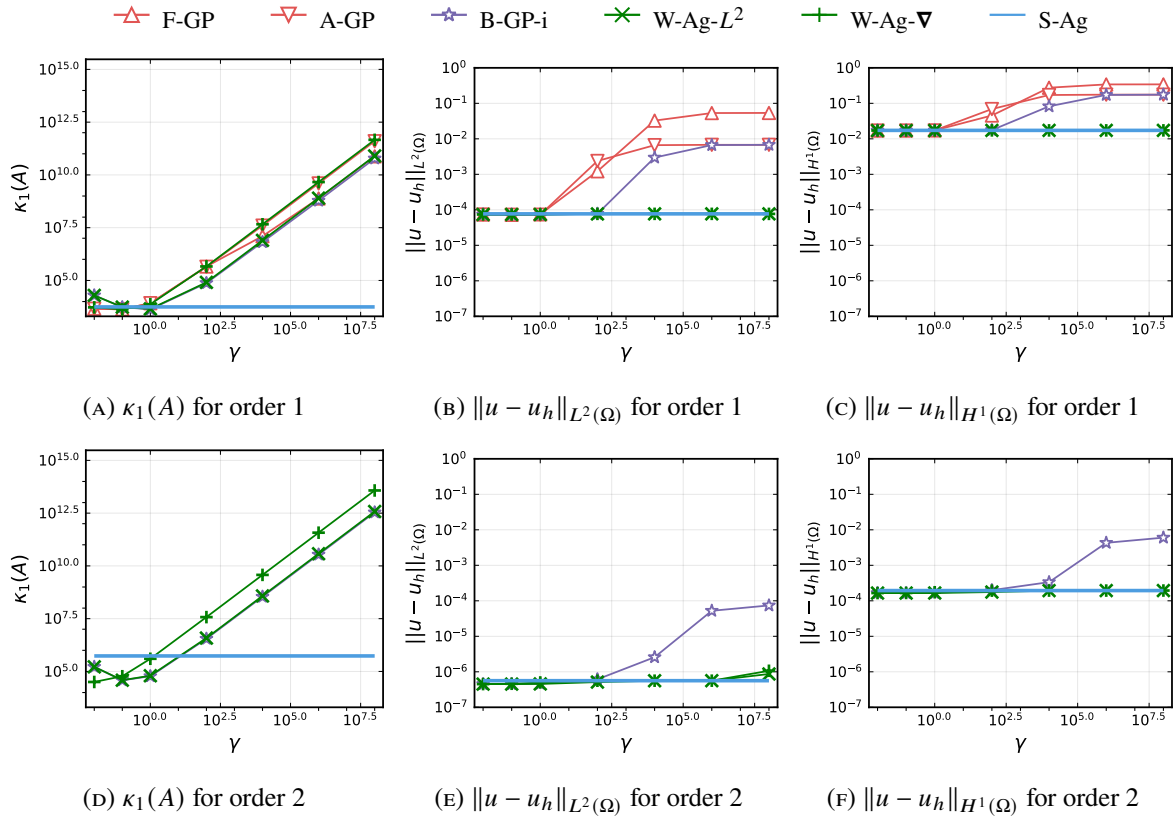


FIGURE 7. Condition number $\kappa_1(A)$, and error norms $\|u - u_h\|_{L^2(\Omega)}$ and $\|u - u_h\|_{H^1(\Omega)}$ vs. penalty parameter γ for the linear elasticity problem with with Neumann and strong Dirichlet boundary conditions on the sphere using linear and quadratic elements in a $40 \times 40 \times 40$ structured tetrahedral mesh.

framework of the Beatriu Pinós Program (Grant Id.: 2016 BP 00145). This work was also supported by computational resources provided by the Australian Government through NCI under the National Computational Merit Allocation Scheme.

REFERENCES

- [1] H. Waisman and L. Berger-Vergiat. An adaptive domain decomposition preconditioner for crack propagation problems modeled by XFEM. *International Journal for Multiscale Computational Engineering*, 11(6):633–654, 2013. doi:[10.1615/IntJMultCompEng.2013006012](https://doi.org/10.1615/IntJMultCompEng.2013006012).
- [2] L. Berger-Vergiat, H. Waisman, B. Hiriyyur, R. Tuminaro, and D. Keyes. Inexact Schwarz-algebraic multigrid preconditioners for crack problems modeled by extended finite element methods. *International Journal for Numerical Methods in Engineering*, 90(3):311–328, 2012. doi:[10.1002/nme.3318](https://doi.org/10.1002/nme.3318).
- [3] B. Schott, C. Ager, and W. A. Wall. Monolithic cut finite element-based approaches for fluid-structure interaction. *International Journal for Numerical Methods in Engineering*, 119(8):757–796, 2019. doi:[10.1002/nme.6072](https://doi.org/10.1002/nme.6072).
- [4] F. Alauzet, B. Fabrèges, M. A. Fernández, and M. Landajuela. Nitsche-XFEM for the coupling of an incompressible fluid with immersed thin-walled structures. *Computer Methods in Applied Mechanics and Engineering*, 301:300–335, 2016. doi:[10.1016/j.cma.2015.12.015](https://doi.org/10.1016/j.cma.2015.12.015).
- [5] S. Zonca, C. Vergara, and L. Formaggia. An unfitted formulation for the interaction of an incompressible fluid with a thick structure via an XFEM/DG approach. *SIAM Journal on Scientific Computing*, 40(1):B59–B84, 2018. doi:[10.1137/16M1097602](https://doi.org/10.1137/16M1097602).
- [6] A. Massing, M. G. Larson, A. Logg, and M. E. Rognes. A Nitsche-based cut finite element method for a fluid-structure interaction problem. *Communications in Applied Mathematics and Computational Science*, 10(2):97–120, 2015. doi:[10.2140/camcos.2015.10.97](https://doi.org/10.2140/camcos.2015.10.97).

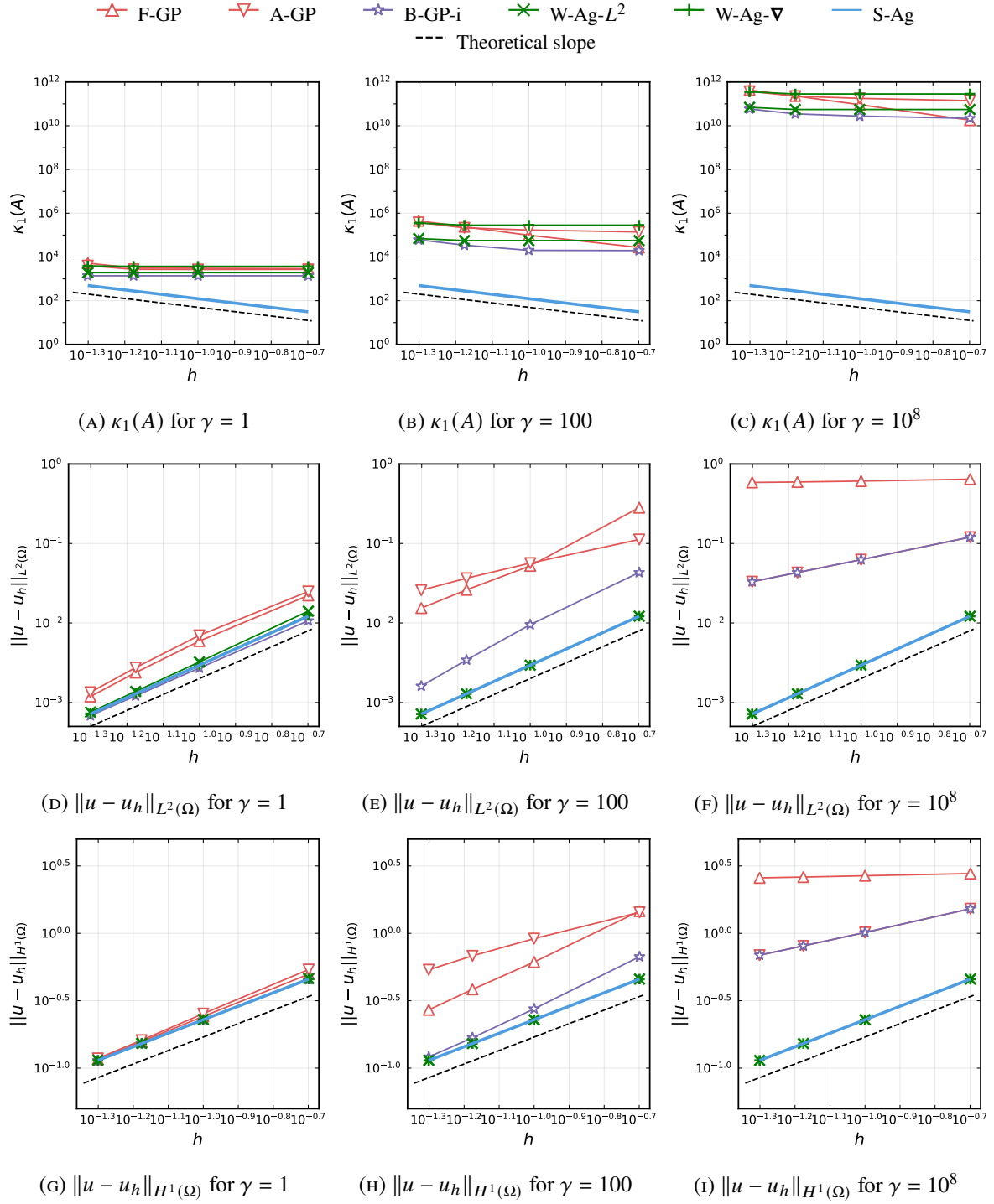


FIGURE 8. Condition number $\kappa_1(A)$, and error norms $\|u - u_h\|_{L^2(\Omega)}$ and $\|u - u_h\|_{H^1(\Omega)}$ vs. mesh size h for the Poisson problem with Nitsche's method on the cube using linear elements. The dashed lines indicate the theoretical bound, i.e., h^{-2} for $\kappa_1(A)$, h^2 for $\|u - u_h\|_{L^2(\Omega)}$ and h for $\|u - u_h\|_{H^1(\Omega)}$.

- [7] H. Sauerland and T. P. Fries. The extended finite element method for two-phase and free-surface flows: A systematic study. *Journal of Computational Physics*, 230(9):3369–3390, 2011. doi:[10.1016/j.jcp.2011.01.033](https://doi.org/10.1016/j.jcp.2011.01.033).
- [8] M. Kirchhart, S. Gross, and A. Reusken. Analysis of an XFEM discretization for Stokes interface problems. *SIAM Journal on Scientific Computing*, 38(2):A1019–A1043, 2016. doi:[10.1137/15M1011779](https://doi.org/10.1137/15M1011779).

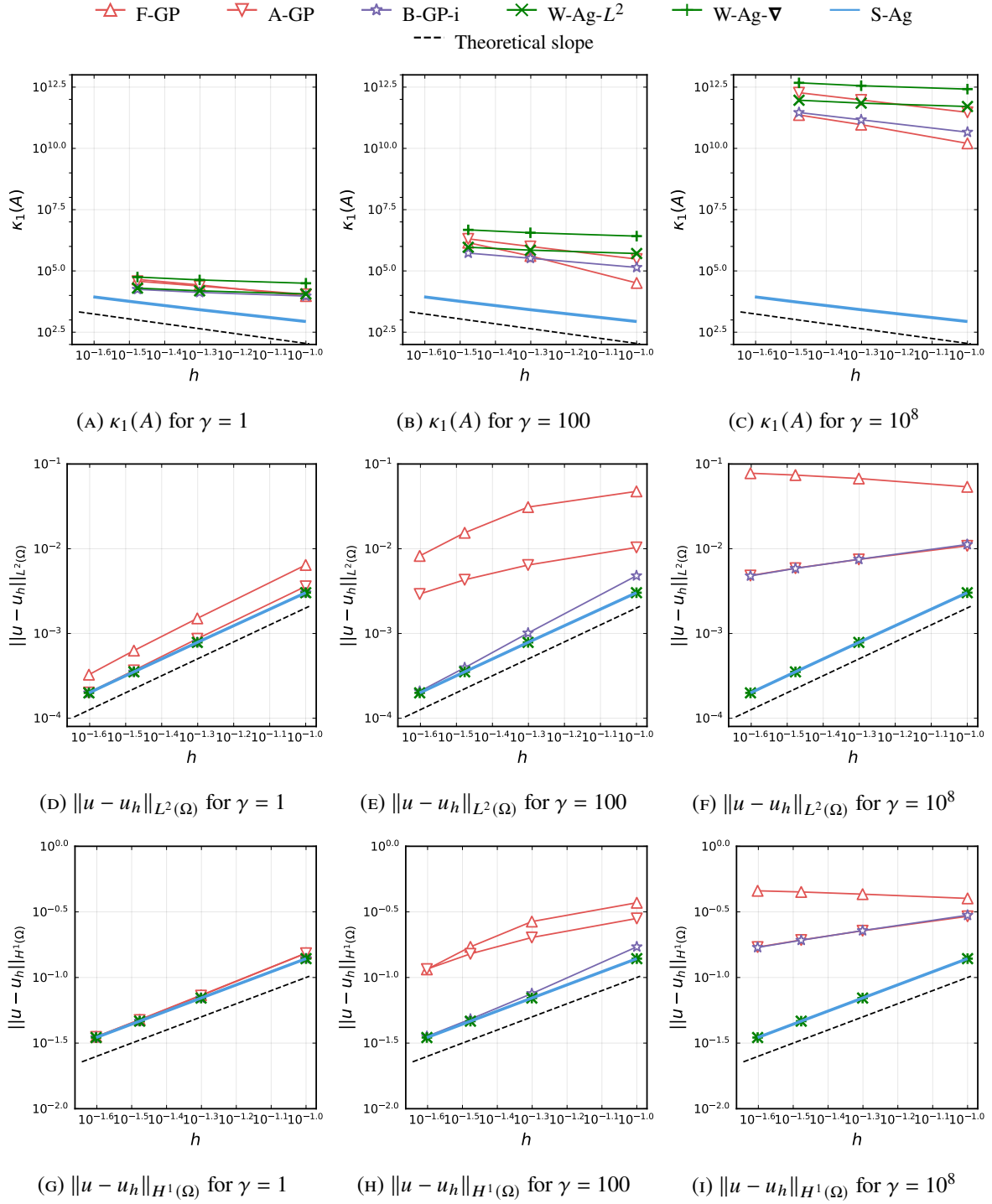


FIGURE 9. Condition number $\kappa_1(A)$, and error norms $\|u - u_h\|_{L^2(\Omega)}$ and $\|u - u_h\|_{H^1(\Omega)}$ vs. mesh size h for the elasticity problem with Neumann boundary conditions on the 8-norm sphere using quadratic elements. The dashed lines indicate the theoretical bound, i.e., h^{-2} for $\kappa_1(A)$, h^3 for $\|u - u_h\|_{L^2(\Omega)}$ and h^2 for $\|u - u_h\|_{H^1(\Omega)}$.

- [9] S. Badia, M. Caicedo, A. F. Martín, and J. Principe. A robust and scalable unfitted adaptive finite element framework for nonlinear solid mechanics. *ArXiv e-prints*, 2020. [arXiv:2012.00280v2](https://arxiv.org/abs/2012.00280v2).
- [10] E. Burman, D. Elfverson, P. Hansbo, M. G. Larson, and K. Larsson. Shape optimization using the cut finite element method. *Computer Methods in Applied Mechanics and Engineering*, 328:242–261, 2018. doi:[10.1016/j.cma.2017.09.005](https://doi.org/10.1016/j.cma.2017.09.005).

- [11] E. Neiva, M. Chiumenti, M. Cervera, E. Salsi, G. Piscopo, S. Badia, A. F. Martín, Z. Chen, C. Lee, and C. Davies. Numerical modelling of heat transfer and experimental validation in powder-bed fusion with the virtual domain approximation. *Finite Elements in Analysis and Design*, 168:103343, 2020. doi:[10.1016/j.finel.2019.103343](https://doi.org/10.1016/j.finel.2019.103343).
- [12] M. Carraturo, J. Jomo, S. Kollmannsberger, A. Reali, F. Auricchio, and E. Rank. Modeling and experimental validation of an immersed thermo-mechanical part-scale analysis for laser powder bed fusion processes. *Additive Manufacturing*, 36:101498, 2020. doi:[10.1016/j.addma.2020.101498](https://doi.org/10.1016/j.addma.2020.101498).
- [13] S. Badia, J. Hampton, and J. Principe. Embedded multilevel monte carlo for uncertainty quantification in random domains. *International Journal for Uncertainty Quantification*, in press. doi:[10.1615/Int.J.UncertaintyQuantification.2021032984](https://doi.org/10.1615/Int.J.UncertaintyQuantification.2021032984).
- [14] T. Belytschko, N. Moës, S. Usui, and C. Parimi. Arbitrary discontinuities in finite elements. *International Journal for Numerical Methods in Engineering*, 50(4):993–1013, 2001. doi:[10.1002/1097-0207\(20010210\)50:4<993::AID-NME164>3.0.CO;2-M](https://doi.org/10.1002/1097-0207(20010210)50:4<993::AID-NME164>3.0.CO;2-M).
- [15] E. Burman, S. Claus, P. Hansbo, M. G. Larson, and A. Massing. CutFEM: Discretizing Geometry and Partial Differential Equations. *International Journal for Numerical Methods in Engineering*, 104(7):472–501, 2015. doi:[10.1002/nme.4823](https://doi.org/10.1002/nme.4823).
- [16] S. Badia, F. Verdugo, and A. F. Martín. The aggregated unfitted finite element method for elliptic problems. *Computer Methods in Applied Mechanics and Engineering*, 336:533–553, 2018. doi:[10.1016/j.cma.2018.03.022](https://doi.org/10.1016/j.cma.2018.03.022).
- [17] D. Elfverson, M. G. Larson, and K. Larsson. CutIGA with basis function removal. *Advanced Modeling and Simulation in Engineering Sciences*, 5(1):6, 2018. doi:[10.1186/s40323-018-0099-2](https://doi.org/10.1186/s40323-018-0099-2).
- [18] R. Mittal and G. Iaccarino. Immersed Boundary Methods. *Annual Review of Fluid Mechanics*, 37(1):239–261, 2005. doi:[10.1146/annurev.fluid.37.061903.175743](https://doi.org/10.1146/annurev.fluid.37.061903.175743).
- [19] D. Schillinger and M. Ruess. The Finite Cell Method: A review in the context of higher-order structural analysis of CAD and image-based geometric models. *Archives of Computational Methods in Engineering*, 22(3):391–455, 2015. doi:[10.1007/s11831-014-9115-y](https://doi.org/10.1007/s11831-014-9115-y).
- [20] A. Main and G. Scovazzi. The Shifted Boundary Method for embedded domain computations. Part I: Poisson and Stokes problems. *Journal of Computational Physics*, 372:972–995, 2018. doi:[10.1016/j.jcp.2017.10.026](https://doi.org/10.1016/j.jcp.2017.10.026).
- [21] D. Kamensky, M.-C. Hsu, D. Schillinger, J. A. Evans, A. Aggarwal, Y. Bazilevs, M. S. Sacks, and T. J. Hughes. An immersogeometric variational framework for fluid–structure interaction: Application to bioprosthetic heart valves. *Computer methods in applied mechanics and engineering*, 284:1005–1053, 2015. doi:[10.1016/j.cma.2014.10.040](https://doi.org/10.1016/j.cma.2014.10.040).
- [22] J. M. Navarro-Jiménez, E. Nadal, M. Tur, J. Martínez-Casas, and J. J. Ródenas. On the use of stabilization techniques in the Cartesian grid finite element method framework for iterative solvers. *International Journal for Numerical Methods in Engineering*, 121(13):3004–3020, 2020. doi:[10.1002/nme.6344](https://doi.org/10.1002/nme.6344).
- [23] R. Saye. Implicit mesh discontinuous Galerkin methods and interfacial gauge methods for high-order accurate interface dynamics, with applications to surface tension dynamics, rigid body fluid–structure interaction, and free surface flow: Part I. *Journal of Computational Physics*, 344:647–682, 2017. doi:[10.1016/j.jcp.2017.04.076](https://doi.org/10.1016/j.jcp.2017.04.076).
- [24] C. Engwer and F. Heimann. Dune-UDG: a cut-cell framework for unfitted discontinuous Galerkin methods. In *Advances in DUNE*, pages 89–100. Springer, 2012. doi:[10.1007/978-3-642-28589-9_7](https://doi.org/10.1007/978-3-642-28589-9_7).
- [25] A. Johansson and M. G. Larson. A high order discontinuous Galerkin Nitsche method for elliptic problems with fictitious boundary. *Numerische Mathematik*, 123(4):607–628, 2013. doi:[10.1007/s00211-012-0497-1](https://doi.org/10.1007/s00211-012-0497-1).
- [26] B. Müller, S. Krämer-Eis, F. Kummer, and M. Oberlack. A high-order discontinuous Galerkin method for compressible flows with immersed boundaries. *International Journal for Numerical Methods in Engineering*, 110(1):3–30, 2017. doi:[10.1002/nme.5343](https://doi.org/10.1002/nme.5343).
- [27] F. de Prenter, C. V. Verhoosel, G. J. van Zwieten, and E. H. van Brummelen. Condition number analysis and preconditioning of the finite cell method. *Computer Methods in Applied Mechanics and Engineering*, 316:297–327, 2017. doi:[10.1016/j.cma.2016.07.006](https://doi.org/10.1016/j.cma.2016.07.006).
- [28] E. Neiva and S. Badia. Robust and scalable h-adaptive aggregated unfitted finite elements for interface elliptic problems. *Computer Methods in Applied Mechanics and Engineering*, 380:113769, July

2021. doi:[10.1016/j.cma.2021.113769](https://doi.org/10.1016/j.cma.2021.113769).
- [29] F. Kummer. Extended discontinuous Galerkin methods for two-phase flows: the spatial discretization. *International Journal for Numerical Methods in Engineering*, 109(2):259–289, 2017. doi:[10.1002/nme.5288](https://doi.org/10.1002/nme.5288).
- [30] C. Lehrenfeld. High order unfitted finite element methods on level set domains using isoparametric mappings. *Computer Methods in Applied Mechanics and Engineering*, 300:716–733, 2016. doi:[10.1016/j.cma.2015.12.005](https://doi.org/10.1016/j.cma.2015.12.005).
- [31] J. Guzmán, M. A. Sánchez, and M. Sarkis. A finite element method for high-contrast interface problems with error estimates independent of contrast. *Journal of Scientific Computing*, 73(1): 330–365, 2017. doi:[10.1007/s10915-017-0415-x](https://doi.org/10.1007/s10915-017-0415-x).
- [32] K. Li, N. M. Atallah, G. A. Main, and G. Scovazzi. The Shifted Interface Method: A flexible approach to embedded interface computations. *International Journal for Numerical Methods in Engineering*, 2019. doi:[10.1002/nme.6231](https://doi.org/10.1002/nme.6231).
- [33] E. Burman. Ghost penalty. *Comptes Rendus Mathématique*, 348(21-22):1217–1220, 2010. doi:[10.1016/j.crma.2010.10.006](https://doi.org/10.1016/j.crma.2010.10.006).
- [34] C. Helzel, M. Berger, and R. Leveque. A high-resolution rotated grid method for conservation laws with embedded geometries. *SIAM Journal on Scientific Computing*, 26(3):785–809, 2005. doi:[10.1137/S106482750343028X](https://doi.org/10.1137/S106482750343028X).
- [35] P. Bastian and C. Engwer. An unfitted finite element method using discontinuous Galerkin. *International journal for numerical methods in engineering*, 79(12):1557–1576, 2009. doi:[10.1002/nme.2631](https://doi.org/10.1002/nme.2631).
- [36] S. Badia, A. F. Martín, and F. Verdugo. Mixed aggregated finite element methods for the unfitted discretization of the Stokes problem. *SIAM Journal on Scientific Computing*, 40(6):B1541–B1576, 2018. doi:[10.1137/18M1185624](https://doi.org/10.1137/18M1185624).
- [37] F. Verdugo, A. F. Martín, and S. Badia. Distributed-memory parallelization of the aggregated unfitted finite element method. *Computer Methods in Applied Mechanics and Engineering*, 357:112583, 2019. doi:[10.1016/j.cma.2019.112583](https://doi.org/10.1016/j.cma.2019.112583).
- [38] S. Badia, A. F. Martín, E. Neiva, and F. Verdugo. The aggregated unfitted finite element method on parallel tree-based adaptive meshes. *SIAM Journal on Scientific Computing*, 43(3):C203–C234, Jan. 2021. doi:[10.1137/20m1344512](https://doi.org/10.1137/20m1344512).
- [39] E. Burman, P. Hansbo, and M. G. Larson. Explicit time stepping for the wave equation using cutfem with discrete extension. *ArXiv e-prints*, 2020. [arXiv:2011.05386](https://arxiv.org/abs/2011.05386).
- [40] J. Nitsche. Über ein Variationsprinzip zur Lösung von Dirichlet-Problemen bei Verwendung von Teilräumen, die keinen Randbedingungen unterworfen sind. *Abhandlungen aus dem Mathematischen Seminar der Universität Hamburg*, 36(1):9–15, 1971. doi:[10.1007/BF02995904](https://doi.org/10.1007/BF02995904).
- [41] J. Freund and R. Stenberg. On weakly imposed boundary conditions for second order problems. In *Finite elements in fluids, Italia, 15-21.10.1995*, pages 327–336. Padovan yliopisto, 1995.
- [42] S. Badia and F. Verdugo. Robust and scalable domain decomposition solvers for unfitted finite element methods. *Journal of Computational and Applied Mathematics*, 344:740–759, 2018. doi:[10.1016/j.cam.2017.09.034](https://doi.org/10.1016/j.cam.2017.09.034).
- [43] E. Burman and P. Hansbo. Fictitious domain finite element methods using cut elements: II. a stabilized nitsche method. *Applied Numerical Mathematics*, 62(4):328–341, Apr. 2012. doi:[10.1016/j.apnum.2011.01.008](https://doi.org/10.1016/j.apnum.2011.01.008).
- [44] P. Hansbo, M. G. Larson, and K. Larsson. Cut Finite Element Methods for Linear Elasticity Problems. In *Geometrically Unfitted Finite Element Methods and Applications*, pages 25–63. Springer, 2017. doi:[10.1007/978-3-319-71431-8_2](https://doi.org/10.1007/978-3-319-71431-8_2).
- [45] A. Hansbo and P. Hansbo. An unfitted finite element method, based on Nitsche’s method, for elliptic interface problems. *Computer methods in applied mechanics and engineering*, 191(47-48): 5537–5552, 2002. doi:[10.1016/S0045-7825\(02\)00524-8](https://doi.org/10.1016/S0045-7825(02)00524-8).
- [46] R. Becker and M. Braack. A finite element pressure gradient stabilization for the Stokes equations based on local projections. *CALCOLO*, 38(4):173–199, 2001. doi:[10.1007/s10092-001-8180-4](https://doi.org/10.1007/s10092-001-8180-4).
- [47] S. Badia. On stabilized finite element methods based on the Scott–Zhang projector. Circumventing the inf–sup condition for the Stokes problem. *Computer Methods in Applied Mechanics and Engineering*, 247-248:65–72, 2012. doi:[10.1016/j.cma.2012.07.020](https://doi.org/10.1016/j.cma.2012.07.020).

- [48] L. R. Scott and S. Zhang. Finite element interpolation of nonsmooth functions satisfying boundary conditions. *Mathematics of Computation*, 54(190):483–483, May 1990. doi:[10.1090/s0025-5718-1990-1011446-7](https://doi.org/10.1090/s0025-5718-1990-1011446-7).
- [49] L. Nguyen, S. Stoter, T. Baum, J. Kirschke, M. Ruess, Z. Yosibash, and D. Schillinger. Phase-field boundary conditions for the voxel finite cell method: Surface-free stress analysis of CT-based bone structures. *International Journal for Numerical Methods in Biomedical Engineering*, 33(12):e2880, 2017. doi:[10.1002/cnm.2880](https://doi.org/10.1002/cnm.2880).
- [50] S. Badia, A. F. Martín, and J. Principe. FEMPAR: An Object-Oriented Parallel Finite Element Framework. *Archives of Computational Methods in Engineering*, 25(2):195–271, 2018. doi:[10.1007/s11831-017-9244-1](https://doi.org/10.1007/s11831-017-9244-1).
- [51] D. Arndt, W. Bangerth, D. Davydov, T. Heister, L. Heltai, M. Kronbichler, M. Maier, J.-P. Pelteret, B. Turcksin, and D. Wells. The deal.II finite element library: Design, features, and insights. *Computers & Mathematics with Applications*, 81:407–422, 2021. doi:[10.1016/j.camwa.2020.02.022](https://doi.org/10.1016/j.camwa.2020.02.022).
- [52] S. Badia and F. Verdugo. Gridap: An extensible Finite Element toolbox in Julia. *Journal of Open Source Software*, 5(52):2520, 2020. doi:[10.21105/joss.02520](https://doi.org/10.21105/joss.02520).
- [53] M. Alnæs, J. Blechta, J. Hake, A. Johansson, B. Kehlet, A. Logg, C. Richardson, J. Ring, M. E. Rognes, and G. N. Wells. The FEniCS Project Version 1.5. *Archive of Numerical Software*, 3(100), 2015. doi:[10.11588/ans.2015.100.20553](https://doi.org/10.11588/ans.2015.100.20553).
- [54] F. de Prenter, C. Lehrenfeld, and A. Massing. A note on the stability parameter in Nitsche’s method for unfitted boundary value problems. *Computers & Mathematics with Applications*, 75(12):4322–4336, 2018. doi:[10.1016/j.camwa.2018.03.032](https://doi.org/10.1016/j.camwa.2018.03.032).
- [55] NCI-Gadi Web site. <https://nci.org.au/our-systems/hpc-systems>. Accessed: 2020-06-22.